Cell Reports

Article

A synthetic chlorophagy receptor promotes plant fitness by mediating chloroplast microautophagy

Graphical abstract

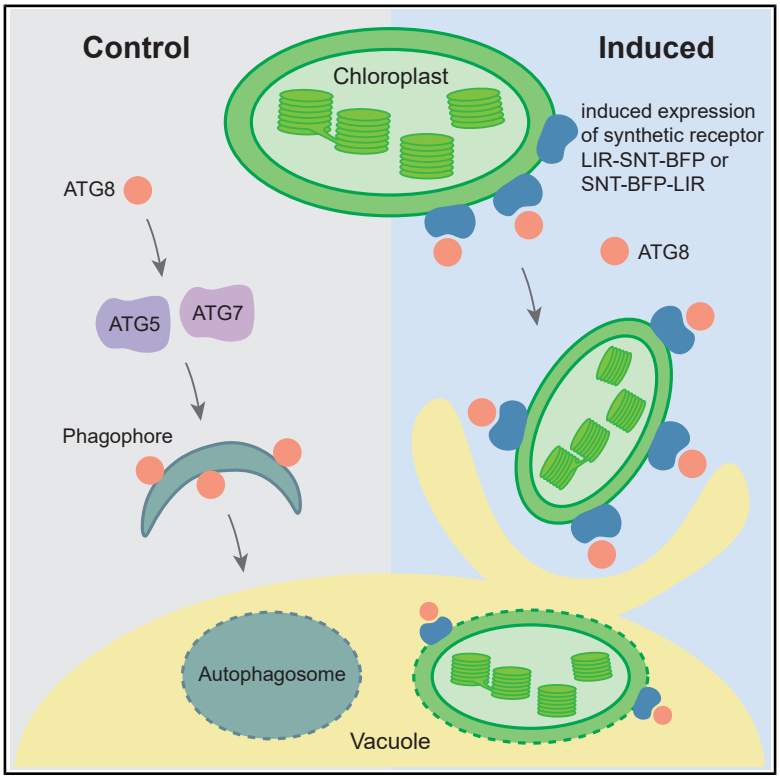

Highlights

- A synthetic chloroplast autophagy receptor, LIR-SNT-BFP, is designed and validated
- Moderately induced chlorophagy promotes growth, whereas excessive chlorophagy inhibits growth
- Induction of chlorophagy stimulates chloroplast division via an unknown mechanism
- ATG8 lipidation is dispensable in induced chloroplast microautophagy

Authors

Rui Liu, Xun Weng, Xinjing Li, ..., Hao Wang, Taotao Wang, Qingqiu Gong

Correspondence

gongqingqiu@sjtu.edu.cn

In brief

Liu et al. design and validate a synthetic chloroplast autophagy receptor that recruits ATG8 to the chloroplasts and promotes both microautophagy of entire chloroplasts and chloroplast division. Moderate induction of this synthetic receptor promotes plant growth but with a clear upper-level limit for the benefits.

Liu et al., 2025, Cell Reports *44*, 115759
June 24, 2025
https://doi.org/10.1016/j.celrep.2025.115759

CellPress

Cell Reports

CellPress
OPEN ACCESS

Article

A synthetic chlorophagy receptor promotes plant fitness by mediating chloroplast microautophagy

Rui Liu,[1] Xun Weng,[2] Xinjing Li,[1] Yongheng Cao,[3] Qiyun Li,[4] Lin Luan,[4] Danqing Tong,[4] Zhaosheng Kong,[3] Hao Wang,[2] Taotao Wang,[1] and Qingqiu Gong[1,5,*]

[1]State Key Laboratory of Microbial Metabolism, Joint International Research Laboratory of Metabolic and Developmental Sciences & Key Laboratory for the Genetics of Developmental and Neuropsychiatric Disorders, School of Life Sciences and Biotechnology, Shanghai Jiao Tong University, Shanghai 200240, P.R. China

[2]Guangdong Provincial Key Laboratory for the Developmental Biology and Environmental Adaption of Agricultural Organisms, College of Life Sciences, South China Agricultural University, Guangzhou, P.R. China

[3]State Key Laboratory of Plant Genomics, Institute of Microbiology, Chinese Academy of Sciences & University of Chinese Academy of Sciences, Beijing 100101, P.R. China

[4]Department of Plant Biology and Ecology, College of Life Sciences, Nankai University, 94 Weijin Road, Tianjin 300071, P.R. China

[5]Lead contact

*Correspondence: gongqingqiu@sjtu.edu.cn

https://doi.org/10.1016/j.celrep.2025.115759

SUMMARY

Chloroplasts are photosynthetic organelles and one of the major protein-containing organelles in green plants and algae. Although chloroplast contents or entire chloroplasts can be cleared by various vesicular pathways and autophagy, canonical chlorophagy receptors remain unidentified. Also, whether chlorophagy can be enhanced to benefit plants remains unknown. Here, we report the design and validation of a synthetic chlorophagy receptor that promotes plant fitness. The receptor LIR-SNT-BFP contains a fragment spanning the LIR/AIM of NBR1 and the N-terminal amphipathic helix of SFR2. The synthetic receptor localizes to chloroplasts and recruits ATG8a *in planta*. Induced expression of the synthetic receptor promotes microautophagy of entire chloroplasts, independent of ATG5 or ATG7. Meanwhile, it induces chloroplast fission. Notably, moderate induction of chlorophagy promotes rosette growth, whereas excessive chlorophagy appears detrimental. Induced chlorophagy also partially suppresses herbicide-induced leaf chlorosis. Our study provides proof of concept for controlling chloroplast degradation using a synthetic chlorophagy receptor.

INTRODUCTION

Eukaryotic cells pack unwanted macromolecules and organelles into double-membraned autophagosomes (macroautophagy) or vacuoles (microautophagy) to maintain homeostasis, and to recycle the building blocks for reuse. Compared with the ubiquitin-26S proteasome pathway and other intracellular degradation pathways that rely on 26S proteasome, autophagy has much larger capacity and less stringent cargo selection.[1] These characteristics make autophagy an ideal platform for the targeted degradation of large objects. In autophagy, the cargoes for degradation are selectively recognized by autophagy receptors/adaptors, such as NBR1 and p62/sequestosome 1 (SQSTM1) in animals, Atg19 in *Saccharomyces cerevisiae*, and NBR1 in Arabidopsis.[2,3] Ubiquitination and protein aggregation are involved in the process of cargo selection. Mechanistically, the LC3-interacting region/ATG8-interacting motif (LIR/AIM) of autophagy receptors, with a consensus [W/F/Y]xx[L/I/V] (x being any amino acid) surrounded by proximal acidic residues, bind two hydrophobic binding pockets in ATG8/LC3s.[4,5] Concurrently, proteins encoded by autophagy-related genes (ATGs) tag the membrane precursor of autophagosome, phagophore/isolation membrane, with ATG8/LC3s, so that autophagy receptors can bring cargoes to phagophores.[6]

Accumulating knowledge of selective autophagy has led to the development of targeted autophagic degradation of proteins and organelles, mainly in mammalian cells and animal models. Autophagosome tethering compounds, identified via high-throughput screening, can bind both LC3s and the target protein, such as mutant huntingtin protein (mHTT), to mediate autophagic degradation of the target protein.[7] Likewise, a compound mT1 binds both the mitochondrial outer membrane protein TSPO and LC3B, thus facilitating the autophagic degradation of damaged mitochondria.[8] One type of autophagy-targeting chimeras (AUTACs) consist of a guanine tag and a specific binder, HaloTag ligand, which binds a target protein fused with a HaloTag. The guanine tag can trigger K63-linked poly-ubiquitination of cargo proteins, which are recognized by cargo receptors for autophagic degradation.[9] Another type of autophagy-targeting chimera (AUTOTAC) is compounds that bind the

autophagy receptor p62. AUTOTAC-bound p62 undergoes conformational changes that exposes its PB1 domain and LIR motif, which facilitates its self-polymerization and LC3 binding, respectively, leading to sequestration and degradation of oncoproteins and aggregates in neurodegeneration.[10] Tethering ATG16L1 or LC3 with ATG16L1-binding peptide (ABP) or LIR can induce targeted degradation of mHTT, and fusion proteins containing mitochondria-targeting sequence of the mitochondrial outer membrane protein TOMM20 plus ABP or LIR promote degradation of damaged mitochondria.[11] Similarly, LIR of Arabidopsis NBR1 can serve as a tool that links targets to ATG8, and this autophagy receptor can facilitate peroxisome degradation in transiently transformed *Nicotiana benthamiana* leaf epidermal cells, and degradation of proteins in Arabidopsis transgenic lines.[12]

The chloroplast is a photosynthetic organelle specific to plants and green algae. The large number (up to 100 per mesophyll cell), size (5–10 μm long, much larger than mitochondria and peroxisomes), and high protein content (RubisCO can account for 50% of total protein) of chloroplasts make them a natural substrate for autophagy and an ideal target of autophagy manipulation in plants. Many forms of chloroplast macroautophagy and microautophagy have been discovered, with various stimuli and substrates identified.[13,14] Several forms require ATG5 and ATG7, the key components of ATG8 conjugation machineries. These machineries include vacuolar degradation of the RubisCO-containing body (RCB), which contains stromal and envelope proteins but not chlorophyll and is triggered by carbon starvation and leaf senescence[15,16]; starch granule-like structure, which contributes to leaf starch degradation[17]; and the ATG8-INTERACTING PROTEIN1-labeled plastid body, which contains thylakoid, stroma, and envelope proteins and is stimulated by leaf senescence, carbon starvation, and salt stress.[18] Apart from the autophagic degradation of chloroplast components or pieces of chloroplasts, damaged entire chloroplasts can be degraded by autophagy, either dependent or independent of ATG5 or ATG7. Entire chloroplasts from individually darkened leaves or photodamaged entire chloroplasts can be transported to the vacuole for degradation, dependent on ATG5 and ATG7.[19–22] In contrast, singlet oxygen-induced chloroplast protrusion into the vacuole, observed in the *plastid ferrochelatase two* mutant, does not require ATG5 or ATG7.[23] NBR1 can be recruited to the surface and interior of photodamaged chloroplasts covered with ubiquitin, and NBR1-decorated chloroplasts are engulfed by the vacuole in a microautophagy-type process (i.e., independent of ATG7).[24,25] In addition to autophagy, senescence-associated vacuoles, which contain stroma and are triggered by leaf senescence,[26–28] and chloroplast vesiculation-containing vesicles, which contain stroma, thylakoid, and envelope proteins and are triggered by senescence as well as salt and oxidative stresses,[29–31] are also forms of vesicle-mediated chloroplast degradation. These discoveries underscore the importance and complexity of chloroplast vesicular degradation and autophagy. So far, a canonical chloroplast autophagy receptor, which presumably localizes to the outer envelope (OE) of chloroplast and recruits ATG8 upon autophagy induction conditions, remains unidentified. Meanwhile, whether chloroplast autophagy can be enhanced, to which degree it can be enhanced, and whether the enhancement can benefit plant growth or stress tolerance, are still open questions.

Here, we addressed these questions by designing and validating an inducible, synthetic chloroplast autophagy receptor. The effects of the induced expression of the synthetic receptor are presented at the sub-cellular, cellular, and organism level. We found that moderate induction of chloroplast autophagy leads to larger rosette sizes. However, the induced autophagy has a clear upper limit for its benefit, beyond which growth inhibition occurs. Additionally, this induced autophagy can partially protect the seedlings from herbicide-induced chlorophyll damage and leaf chlorosis. This form of chloroplast autophagy appears to be a type of microautophagy, as it is independent of the ATG8 conjugation machinery, specifically ATG5 and ATG7, and its association with striking changes in vacuole dynamics. Interestingly, this induced chloroplast autophagy is accompanied by chloroplast fission. However, induced chloroplast autophagy was still observed in the *pdv2* mutant, which is characterized by giant chloroplasts. These observations led us to speculate that a novel form of microautophagy may be responsible for this chloroplast degradation.

RESULTS

Design and validation of a synthetic chloroplast autophagy receptor

A functional synthetic chloroplast autophagy receptor is expected to localize to the outer envelope (OE) of the chloroplast and recruit ATG8 once expressed. To achieve this, we cloned a fragment containing the LIR/AIM of Arabidopsis NBR1 (Figure S1A), the well-characterized selective autophagy receptor/adaptor.[32] Then, we cloned the N-terminal amphipathic α-helix (SNT) of SENSITIVE TO FREEZING 2 (SFR2) (Figures S1B and S1C), which targets to the OE of chloroplast[33] and fused it after LIR. For imaging, a blue fluorescent protein (BFP) tag was fused in frame after SNT (Figure 1A). The fusion protein LIR-SNT-BFP coated the chloroplast and colocalized with ATG8a in transiently transformed *N. benthamiana* leaf epidermal cells (Figure 1B) and in transiently transformed Arabidopsis mesophyll protoplasts (Figure 1C). For inducible expression in transgenic Arabidopsis, a glucocorticoid receptor-based inducible gene expression system (*GVG*) was fused in frame before the receptor,[34] resulting in *GVG:LIR-SNT-BFP*, the inducible synthetic chlorophagy receptor (Figure 1A).

We transformed an autophagy marker line, *ProUBQ10:GFP-ATG8a* (*GFP-ATG8a*),[35] with the synthetic chlorophagy receptor and obtained T3 transgenic lines that carry both *GFP-ATG8a* and *GVG:LIR-SNT-BFP* (Figures S2A and S2B). We also obtained T3 transgenic lines carrying *GFP-ATG8a* and *GVG:SNT-BFP*, which serve as a negative control (Figures S2A and S2B). To preclude lines with T-DNA insertion in photosynthetic genes, T-DNA insertion sites in individual lines were determined by thermal asymmetric interlaced-PCR (Figures S2C and S2D). Line 1, line 2, and line 27 were used in most experiments, for they have intergenic T-DNA insertions, and relatively stable dexamethasone (DEX)-induced expression of the receptor.

We found that BFP signals quench easily during confocal imaging in stable transgenic lines. Therefore, we took a biochemical approach to validate that the synthetic chlorophagy receptor

CellPress
OPEN ACCESS

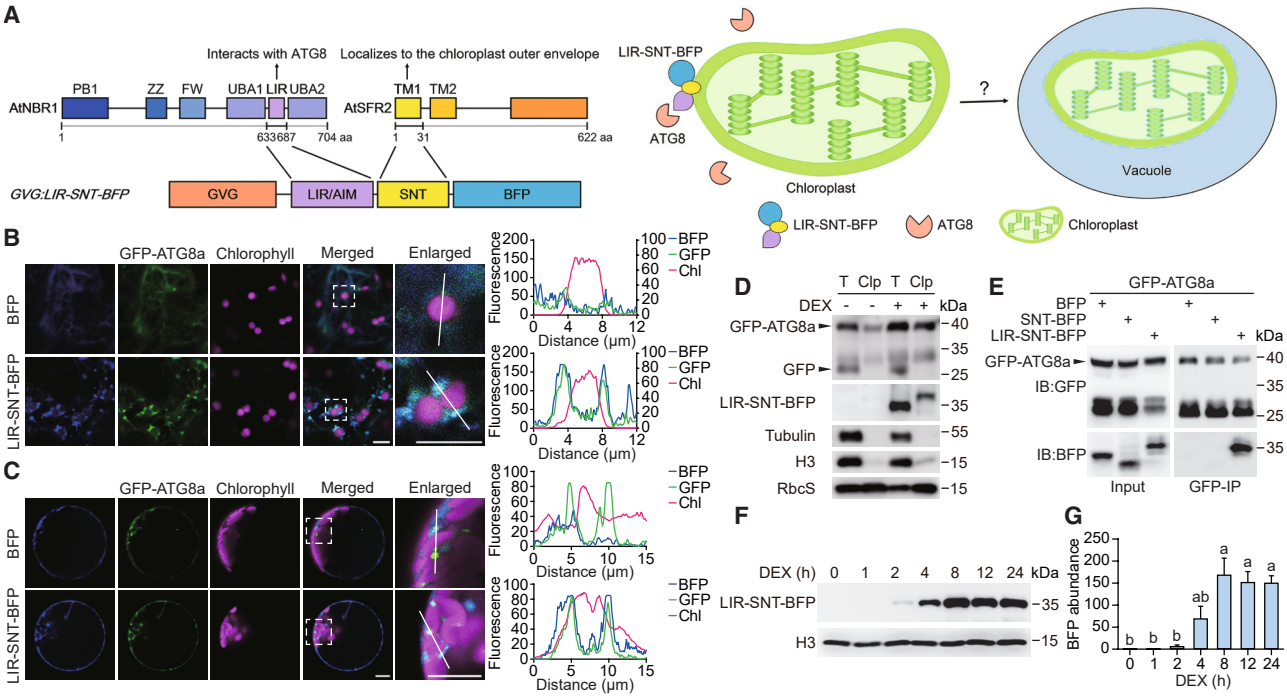

Figure 1. Development of a synthetic chloroplast autophagy receptor

(A) Diagram of the synthetic chlorophagy receptor. The synthetic receptor LIR-SNT-BFP comprises the LIR/AIM from AtNBR1 (LIR/AIM, amino acids [aa] 633–687), the N-terminal amphipathic helix of AtSFR2 (SNT, aa 1–31), and a fluorescent protein BFP, fused in frame after a glucocorticoid receptor-based inducible gene expression system (*GVG*). LIR-SNT-BFP is expected to localize to the outer envelope (OE) of chloroplasts, where it recruits ATG8 to facilitate autophagic degradation of chloroplasts, following dexamethasone (DEX) treatment.

(B) The synthetic chlorophagy receptor LIR-SNT-BFP coats chloroplasts and colocalizes with ATG8a in transiently transformed tobacco. *N. benthamiana* leaf epidermal cells transiently co-expressing GFP-ATG8a and BFP or LIR-SNT-BFP were analyzed by confocal microscopy. Scale bar, 10 μm.

(C) LIR-SNT-BFP coats chloroplasts and colocalizes with ATG8a in transiently transformed Arabidopsis protoplasts. Mesophyll protoplasts prepared from 4-week-old *GFP-ATG8a* plants were transiently transformed with BFP or LIR-SNT-BFP and analyzed by confocal microscopy. Scale bar, 10 μm. The colocalization was determined by calculating fluorescence intensity along the white lines in (B) and (C).

(D) Western blot (WB) analysis of LIR-SNT-BFP and GFP-ATG8a on purified chloroplasts. Total proteins (T) and purified chloroplasts proteins (Clp) of the transgenic Arabidopsis expressing *GFP-ATG8a/LIR-SNT-BFP*, treated with DMSO or 30 μM DEX, were analyzed. Antibodies toward GFP, BFP, tubulin (cytoplasm marker), histone H3 (H3, nucleus marker), and RubisCO small subunit (RbcS, chloroplast marker) were used.

(E) coIP assay showing the *in vivo* interaction between GFP-ATG8a and LIR-SNT-BFP. Transgenic lines co-expressing *GFP-ATG8a* and *BFP*, *SNT-BFP*, or *LIR-SNT-BFP* were treated with 30 μM DEX before coIP. Proteins were immunoprecipitated with GFP-Trap beads and detected with anti-GFP and anti-BFP.

(F) DEX-induced expression of LIR-SNT-BFP. Fourteen-day-old transgenic seedlings expressing *GFP-ATG8a/LIR-SNT-BFP* were treated with 30 μM DEX, harvested at indicated time points, and analyzed by WB. Anti-BFP was used to detect LIR-SNT-BFP. H3 served as an internal control.

(G) Band intensities of LIR-SNT-BFP in (F) were quantified and normalized to H3.

Data are means ± SEMs of three biological replicates. Different letters denote statistically significant differences ($p < 0.05$) using Tukey's honestly significant difference (HSD) test. Representative images or WBs from three biological replicates are shown in (B)–(F).

can recruit ATG8 to the chloroplasts. Chloroplasts from the transgenic lines were purified with differential centrifugation and Percoll gradient centrifugation, and the presence of LIR-SNT-BFP and GFP-ATG8a on the purified chloroplasts after DEX induction was verified with western blotting (WB; Figure 1D). Notably, ATG8a was detected on the purified chloroplasts before DEX induction (Figure 1D), which is in line with a previous report.[36] The interaction between ATG8a and the synthetic chlorophagy receptor was verified with co-immunoprecipitation (coIP) (Figure 1E). Neither BFP nor SNT-BFP but LIR-SNT-BFP interact with GFP-ATG8a in the double transgenic lines co-expressing the *GFP-ATG8a* and *BFP*-tagged proteins (Figure 1E). The DEX-induced expression of the synthetic chlorophagy receptor starts from 4 h, and can be steadily observed after 8 h (Figures 1F and 1G).

The synthetic chlorophagy receptor facilitates autophagic degradation of chloroplast proteins

To see whether and how the DEX-induced expression of the synthetic receptor may induce chloroplast autophagy, we examined the GFP signals in the mesophyll cells of mock- and DEX-treated *GFP-ATG8a/LIR-SNT-BFP* seedlings. Seedlings carrying *GFP-ATG8a/SNT-BFP* served as a negative control. In line with the WB results (Figure 1D), and as reported before,[36] GFP-ATG8a can be seen on the surface of chloroplasts (Figure 2A). Treating *GFP-ATG8a/LIR-SNT-BFP* with DEX induced a 5-fold accumulation of GFP-ATG8a puncta on chloroplasts, which was not observed in *GFP-ATG8a/SNT-BFP* (Figures 2A and 2B), validating the effective recruitment of ATG8 by the synthetic receptor. Consistently, by tracking the autophagic flux with GFP-ATG8

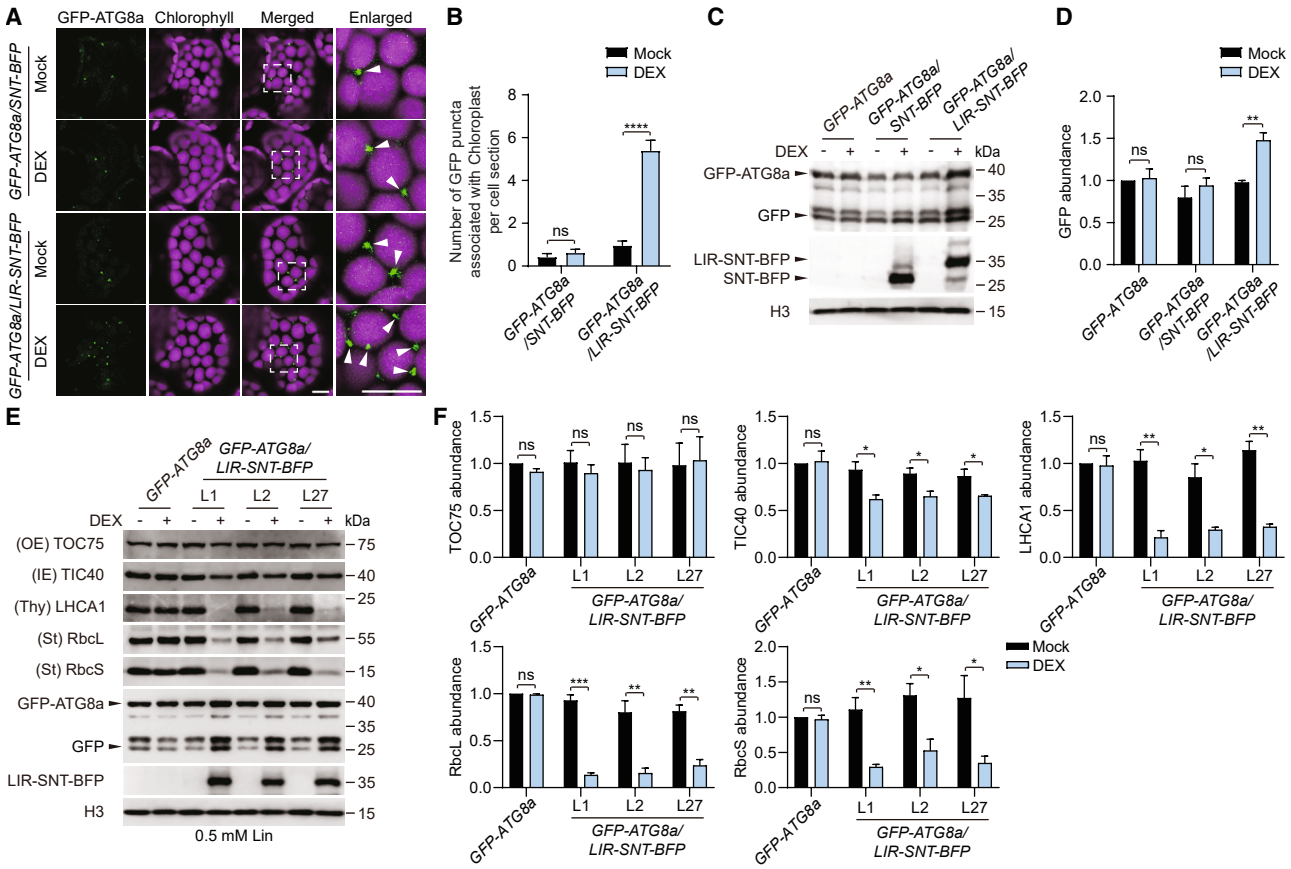

Figure 2. The synthetic chlorophagy receptor facilitates autophagic degradation of chloroplasts

(A) Expression of LIR-SNT-BFP but not SNT-BFP promotes GFP-ATG8a recruitment to the chloroplast. Five-day-old seedlings expressing *LIR-SNT-BFP* or *SNT-BFP* in the *GFP-ATG8a* background were treated with DMSO or 10 μM DEX for 3 days, before confocal imaging. White arrowheads indicate clusters of GFP-ATG8a on chloroplasts. Scale bar, 10 μm.

(B) Quantification of the number of GFP puncta associated with chloroplasts per cell section in (A). Data are means ± SEMs (n = 35).

(C) Autophagy is induced by induction of LIR-SNT-BFP. Five-day-old seedlings expressing *LIR-SNT-BFP* or *SNT-BFP* in the *GFP-ATG8a* background were treated with DMSO or 10 μM DEX for 10 days before WB analysis of GFP cleavage from GFP-ATG8a, indicative of autophagic flux. Anti-GFP and anti-BFP were used to detect GFP-ATG8a, free GFP, LIR-SNT-BFP, and SNT-BFP. H3 served as an internal control.

(D) Band intensities of free GFP in (C) were quantified and normalized to H3.

(E) LIR-SNT-BFP promotes the degradation of chloroplast proteins in the presence of lincomycin (Lin), an inhibitor of chloroplast protein synthesis. Five-day-old seedlings expressing *LIR-SNT-BFP* in the *GFP-ATG8a* background were treated with DMSO or 10 μM DEX plus 0.5 mM Lin for 14 days, before WB detection of chloroplast proteins TOC75 (chloroplast OE protein), TIC40 (IE protein), LHCA1 (thylakoid [Thy] protein), RbcL (chloroplast-encoded stromal [St] protein), and RbcS (St protein). Anti-GFP and anti-BFP were used to detect GFP-ATG8a and LIR-SNT-BFP. H3 served as an internal control.

(F) Band intensities in (E) were quantified and normalized to H3. *GFP-ATG8a* in DMSO (DEX-) was set as 100%.

Data are means ± SEMs of three biological replicates. *p < 0.05; **p < 0.01; ***p < 0.001; ****p < 0.0001; ns, no significant difference (Student's t test). Representative images or WBs from three biological replicates are shown in (A), (C), and (E).

cleavage assay (Figure 2C), we showed that autophagy was significantly induced upon LIR-SNT-BFP accumulation, but stayed unchanged in DEX-treated *GFP-ATG8a* or *GFP-ATG8a/SNT-BFP* seedlings (Figures 2C and 2D).

To see whether the chloroplasts were degraded as a consequence of induced autophagy, we compared the levels of chloroplast proteins that localize to the outer envelope (OE; TOC75), inner envelope (IE; TIC40), thylakoids (LHCA1), and stroma (RbcL and RbcS), before and after DEX induction. The levels of chloroplast proteins examined were almost unchanged after DEX induction (Figures S3A and S3B). We reasoned that the degradation of chloroplast proteins could have been masked by new protein synthesis, hence treated the plants with lincomycin, a lincosamide antibiotic that specifically inhibits chloroplast protein translation.[37] Indeed, except for TOC75, whose level is reported to be regulated by NBR1-mediated selective autophagy,[36] levels of chloroplast inner membrane proteins, thylakoid proteins, and stromal proteins were significantly reduced by synthetic receptor induction in the presence of lincomycin (Figures 2E and 2F).

To further validate that the amphipathic α-helix of SFR2 (SNT) can mediate chloroplast targeting and membrane binding of LIR, we generated an alternative synthetic receptor, *GVG:SNT-BFP-LIR*, by fusing LIR after rather than before SNT and obtained transgenic lines as for *GVG:LIR-SNT-BFP*. As with the original receptor,

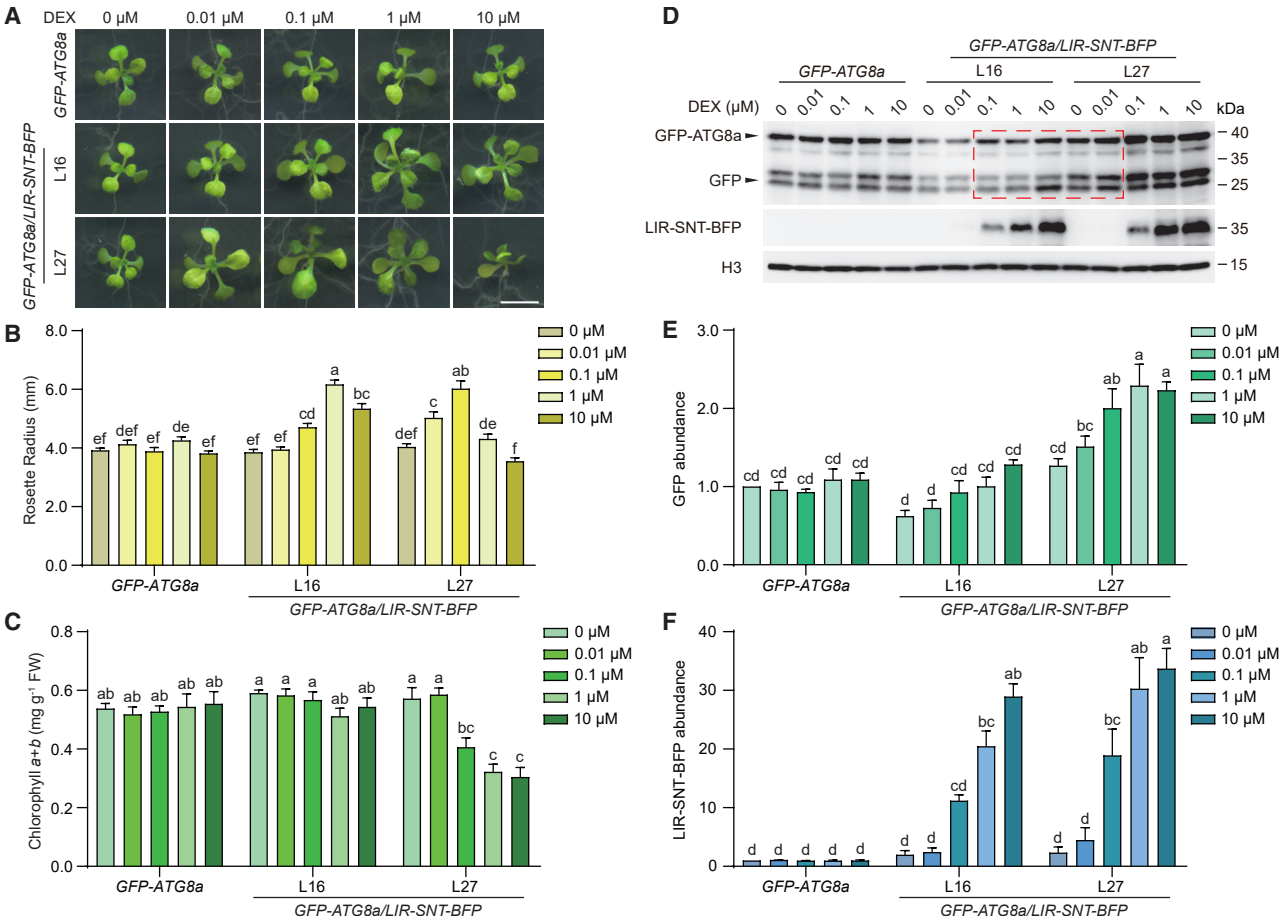

Figure 3. Moderate induction of the synthetic chlorophagy receptor promotes plant growth, whereas excessive induction inhibits plant growth

(A) Five-day-old seedlings expressing *LIR-SNT-BFP* in the *GFP-ATG8a* background were treated with indicated concentrations of DEX for 10 days. Scale bar, 5 mm.

(B) Rosette radius measured from plants in (A). Data are means ± SEMs (n = 16).

(C) Chlorophyll contents of plants in (A). Data are means ± SEMs (n = 20).

(D) Autophagic flux increment roughly correlates to accumulation of LIR-SNT-BFP. Total proteins were extracted from plants in (A). Anti-GFP and anti-BFP were used to detect GFP-ATG8a, free GFP, and LIR-SNT-BFP. H3 served as an internal control.

(E) Band intensities of free GFP indicated the level of autophagic flux in (D) were quantified and normalized to H3.

(F) Band intensities of LIR-SNT-BFP induced by DEX treatment in (D) were quantified and normalized to H3. *GFP-ATG8a* in DMSO (DEX-) was set as 100%. Data are means ± SEM of three biological replicates. Different letters indicate statistically significant differences ($p < 0.05$), as determined with a Tukey's HSD test. Representative images or WBs from three biological replicates are shown in (A) and (D).

this receptor interacted with ATG8a *in vivo* (Figure S4A). The alternative receptor responded similarly to DEX induction and led to the degradation of LHCA1 and RbcL (Figures S4B–S4D). These observations confirmed that LIR can be fused to either side of the amphipathic α-helix of SFR2 to elicit chlorophagy, although the C-terminal fusion of LIR appeared to be less effective.

Moderate induction of the synthetic receptor promotes plant growth and partially protects leaves from herbicides

Previous studies have revealed the critical role of chlorophagy in protecting plants from adverse environmental conditions, such as prolonged carbon starvation, photodamage, heat, or UVB.[14] Nevertheless, it remains unknown whether induced chlorophagy, in a certain range, can enhance plant growth. We took advantage of the inducible expression of the synthetic receptor and treated *GFP-ATG8a/LIR-SNT-BFP* lines with 0.01–10 μM DEX for 10 days to compare their rosette sizes. For line 16, in which the synthetic receptor accumulated to a lower level (Figures S2A and S2B), 0.1–10 μM DEX led to larger rosette. For line 27, in which the synthetic receptor was highly expressed (Figures S2A and S2B), 0.01–0.1 μM DEX treatments increased the rosette size; however, 1–10 μM DEX treatment led to reduced rosette size (Figures 3A and 3B). In addition, line 27, treated with 0.1–10 μM DEX, had reduced chlorophyll contents (Figure 3C). We examined the autophagic fluxes and the expression levels of the synthetic receptor in these plants. A positive correlation between the expression level of the synthetic receptor and the level of

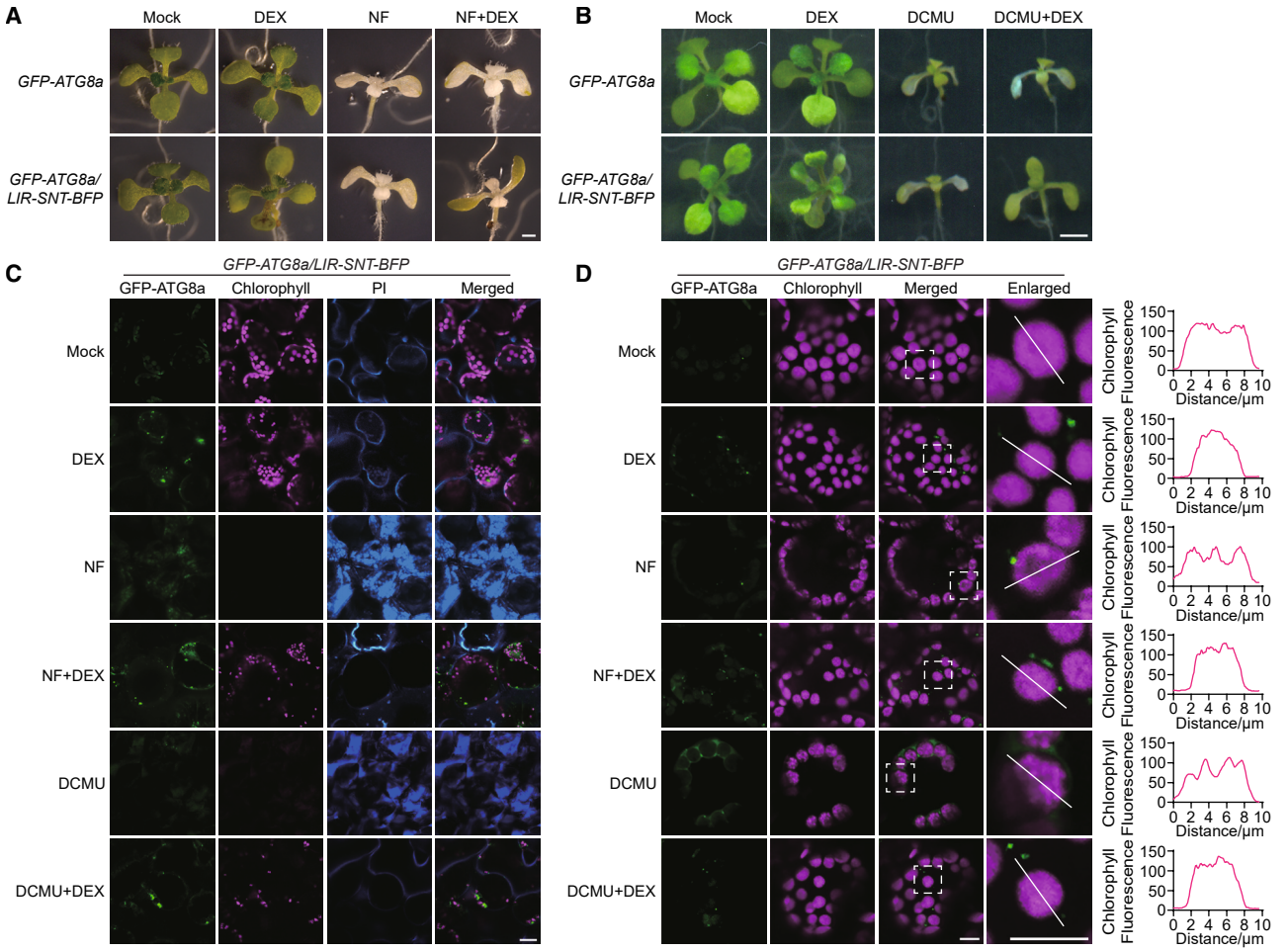

Figure 4. Induction of the synthetic chlorophagy receptor partially protects plant from herbicides norflurazon (NF) and DCMU

(A) NF led to leaf chlorosis, whereas LIR-SNT-BFP induction partially protected cotyledons from chlorosis. Five-day-old seedlings expressing *LIR-SNT-BFP* in the *GFP-ATG8a* background were treated with 10 μM DEX, 1 μM NF, or DEX plus NF for 7 days. Scale bar, 1 mm.

(B) DCMU led to leaf chlorosis, whereas LIR-SNT-BFP induction partially protected cotyledons from chlorosis. Five-day-old seedlings expressing *LIR-SNT-BFP* in the *GFP-ATG8a* background were treated with 10 μM DEX, 2 μM DCMU, or DEX plus DCMU for 10 days. Scale bar, 2 mm.

(C) NF- or DCMU-induced chlorophyll loss and cell death were partially suppressed by LIR-SNT-BFP induction. Five-day-old seedlings expressing *GFP-ATG8a/LIR-SNT-BFP* were treated with 10 μM DEX, 1 μM NF, 2 μM DCMU, or combinations of the chemicals as indicated for 10 days, before confocal imaging. Cell death was visualized by staining with propidium iodine (PI). Scale bar, 20 μm.

(D) NF- or DCMU-induced abnormal, uneven distribution of chlorophyll was partially recovered by LIR-SNT-BFP induction. Five-day-old seedlings expressing *GFP-ATG8a/LIR-SNT-BFP* were treated with 10 μM DEX, 1 μM NF, 10 μM DCMU, or combinations of the chemicals as indicated for 3 days, before confocal imaging. Chlorophyll fluorescence along the white lines plotted to the right. Scale bar, 10 μm.

Representative images from three biological replicates are shown in (A)–(D).

autophagy indicated by the increment of free GFP processed from GFP-ATG8a was observed (Figures 3D–3F). We also found that when the synthetic receptor is induced to a certain level range, which corresponds to 0.1–10 μM DEX in line 16 and 0–0.01 μM DEX in line 27, plant growth is promoted to a similar extent. When the synthetic receptor accumulated beyond this level, plant growth is inhibited, and the chlorophyll content drops (Figures 3A–3F). Clearly, in a certain range, plant growth correlates with the expression level of the synthetic chlorophagy receptor and the level of autophagy.

We reasoned that artificially induced chlorophagy might accelerate the removal of damaged chloroplast components; thus, it might help alleviate the damage caused by certain herbicides. We tested *GFP-ATG8a/LIR-SNT-BFP* plants on norflurazon (NF), a pyridazinone herbicide that disrupts carotenoid synthesis,[38] and 3-(3,4-dichlorophenyl)-1,1-dimethylurea (DCMU), a herbicide of the arylurea class that inhibits photosynthetic electron transport.[39] Both NF and DCMU led to photobleaching of cotyledons in *GFP-ATG8a* and *GFP-ATG8a/LIR-SNT-BFP*. In contrast, DEX induction of the synthetic chlorophagy receptor partially reduced the chlorosis (Figures 4A and 4B). Confocal microscopy confirmed the reduced cell death, indicated by propidium iodide (PI) staining, and reduced chlorophyll loss caused by NF or DCMU in DEX-treated plants expressing

GFP-ATG8a/LIR-SNT-BFP (Figure 4C) but not in the plants expressing *GFP-ATG8a* (Figure S5A). In particular, the uneven distribution of chlorophyll caused by NF or DCMU, indicative of defective chloroplast structure and function, was partially restored in DEX-treated plants expressing *GFP-ATG8a/LIR-SNT-BFP* (Figure 4D) but not in the control line *GFP-ATG8a* (Figure S5B). In seedlings grown in soil, we also observed partial suppression of NF-induced plant death by induced expression of the synthetic chlorophagy receptor (Figure S5C). We concluded that artificially induced chloroplast autophagy, which likely exceeds the level of endogenous chlorophagy, can help maintain chloroplast homeostasis when chlorophyll synthesis or electron transport is compromised by certain herbicides.

Induction of the synthetic receptor promotes chloroplast division

In animals and yeasts, long tubular mitochondria divide before they can be engulfed by autophagosomes.[40,41] Chloroplasts are much larger than mitochondria, and various forms of chloroplast piecemeal autophagy, as well as microautophagy of the entire chloroplasts, have been reported.[14,16] Still, the relationship between chloroplast division and autophagy is largely unknown. Since the chloroplasts became smaller in DEX-treated *GFP-ATG8a/LIR-SNT-BFP* plants (Figure 4D), we asked whether chloroplasts divide before they are degraded in the vacuole. Following the methods in chloroplast division studies,[42,43] we quantified the numbers of chloroplasts per mesophyll cell in mock- and DEX-treated *GFP-ATG8a/LIR-SNT-BFP* plants and saw significant increments in all DEX-treated lines that could be a consequence of chloroplast division (Figures 5A and 5B). Indeed, we observed more dumbbell-shaped chloroplasts that appear to be undergoing fission in DEX-treated *GFP-ATG8a/LIR-SNT-BFP* mesophyll cells (Figures 5C and 5D). Then, to see whether known machineries mediate the division, we examined the protein expression level of PLASTID DIVISION2 (PDV2) in transgenic plants. PDV2 is a land plant-specific integral OE membrane protein that has a positive dosage effect on chloroplast division.[44,45] Mechanistically, PDV2 recruits the cytosolic dynamin-related protein DRP5B/ARC5 to the division site to complete chloroplast division.[45,46] To our surprise, despite the increased chloroplast numbers, the protein level of PDV2 stayed unchanged in DEX-treated *GFP-ATG8a/LIR-SNT-BFP* plants (Figures 5E and 5F). We then crossed the *pdv2* mutant into *GFP-ATG8a/LIR-SNT-BFP*. Confocal imaging and transmission electron microscopy (TEM) showed that the giant chloroplast phenotype in *pdv2/GFP-ATG8a/LIR-SNT-BFP* stayed unchanged after DEX treatment (Figures 5G and 5H). However, DEX-induced chloroplast protein degradation in *pdv2/GFP-ATG8a/LIR-SNT-BFP* was similar to what we observed in *GFP-ATG8a/LIR-SNT-BFP* (Figures 5I and 5J). Likewise, the synthetic chlorophagy receptor partially protected *pdv2* from NF (Figures S6A and S6B). These results indicated that the giant chloroplasts in *pdv2* could still undergo synthetic receptor-elicited chlorophagy. Therefore, PDV2-mediated chloroplast division does not seem to be required for this specific form of chlorophagy.

The synthetic receptor-elicited chlorophagy does not require the ATG8 conjugation machinery proteins ATG5 and ATG7

To gain more insight into the chloroplast autophagy elicited by the synthetic receptor, we crossed three autophagy-deficient mutants, *atg2*, *atg5*, and *atg7*, into *GFP-ATG8a/LIR-SNT-BFP*. ATG2 is a lipid transfer protein key to phagophore expansion and autophagosome closure[47]; ATG5 and ATG7 are required for ATG8 conjugation.[48] We obtained *atg5/GFP-ATG8a/LIR-SNT-BFP* and *atg7/GFP-ATG8a/LIR-SNT-BFP* lines but failed to recover lines that can express the synthetic receptor in the *atg2* background (Figures S7A–S7C). Interestingly, the DEX-induced synthetic receptor partially rescued the photobleaching and uneven distribution of chlorophyll in NF-treated *atg5/GFP-ATG8a/LIR-SNT-BFP* and *atg7/GFP-ATG8a/LIR-SNT-BFP*, as in *GFP-ATG8a/LIR-SNT-BFP* (Figures 6A and 6B). Consistent with this, DEX-induced chloroplast protein degradation in *atg5* and *atg7* in the presence of lincomycin was comparable to the wild-type background (Figures 6C and 6D). Reduced chloroplast sizes upon DEX treatment were also observed in *atg5* and *atg7* as in the wild-type background (Figures S7D and S7E). All these observations indicated that ATG5 and ATG7, key components of the ATG8 conjugation machinery, are dispensable for this specific form of chloroplast autophagy.

The synthetic receptor-elicited chlorophagy is likely a form of microautophagy

We speculated that ATG5- and ATG7-independent synthetic receptor-mediated chlorophagy may be a form of microautophagy, with the lytic vacuoles devouring the chloroplasts. To explore this possibility, we introduced a tonoplast marker, *YFP-VAMP711*,[49] into *GFP-ATG8a/LIR-SNT-BFP* by crossing and examined the relationship between chloroplasts and vacuoles with confocal imaging. Indeed, tonoplast invaginations surrounding individual chloroplasts increased by approximately 2-fold after DEX induction in mesophyll cells and in protoplasts prepared from this triple transgenic line (Figures 7A–7D). We then employed live-cell imaging to capture the dynamic interaction between the chloroplasts and the vacuoles. Without DEX-induction of the synthetic chlorophagy receptor, the tonoplast surrounding the chloroplasts was relatively quiet, with sporadic *trans*-strands observed (Figure 7E; Videos S1 and S2). After DEX-induced expression of LIR-SNT-BFP, however, the tonoplast became highly dynamic and actively chased chloroplasts and wrapped around them (Figure 7E; Videos S3 and S4). Chloroplasts wrapped in vacuoles were observed frequently after DEX treatment, and small vacuoles were often seen beside the chloroplasts, likely resulting from vacuole fission after invagination of chloroplasts (Figure 7F; Video S4).

We also generated stable transgenic lines carrying *RBCS1A-mCherry/GFP-ATG8a/LIR-SNT-BFP* to document chloroplast degradation by looking at RBCS1A-mCherry. We found that entire chloroplasts, instead of mCherry-labeled puncta that represent RCB, accumulated in the vacuole after DEX-induction of LIR-SNT-BFP (Figures 7G and 7H). Similarly, TEM analyses showed that the number of chloroplasts in the vacuoles largely increased in the mesophyll cells of *GFP-ATG8a/LIR-SNT-BFP* after DEX treatment (Figures 7I and 7J). We further performed

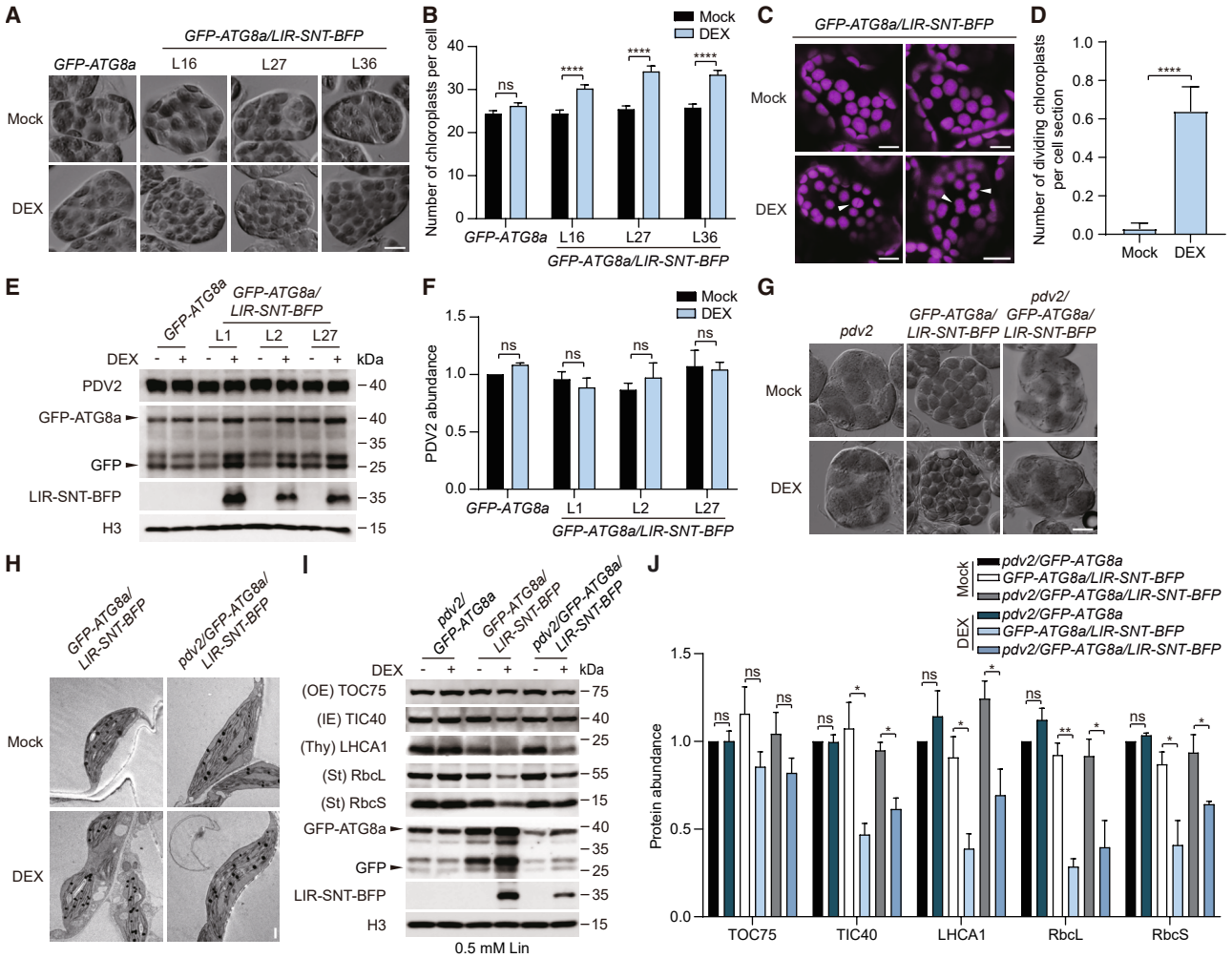

Figure 5. Induction of the synthetic chlorophagy receptor stimulates chloroplast division

(A) Induction of LIR-SNT-BFP significantly increases the number of chloroplasts per cell. Five-day-old seedlings expressing *LIR-SNT-BFP* in the *GFP-ATG8a* background were treated with DMSO or 10 μM DEX for 10 days. Mesophyll cells from the first pair of true leaves were fixed before confocal imaging. Scale bar, 10 μm.

(B) Quantification of the number of chloroplasts per cell in (A). Data are means ± SEMs (n = 30).

(C) Induction of LIR-SNT-BFP significantly increases the incidence of chloroplast division per cell section. Five-day-old seedlings expressing *GFP-ATG8a/LIR-SNT-BFP* were treated with DMSO or 10 μM DEX for 5 days before confocal imaging. White arrowheads indicate dividing chloroplasts. Scale bar, 10 μm.

(D) Quantification of the number of dividing chloroplasts per cell section in (C). Data are means ± SEMs (n = 36).

(E) PDV2 protein levels remained unchanged before and after LIR-SNT-BFP induction. Five-day-old seedlings expressing *LIR-SNT-BFP* in the *GFP-ATG8a* background were treated with DMSO or 10 μM DEX for 10 days before WB analysis. Proteins were detected by anti-PDV2, anti-GFP, and anti-BFP. H3 served as an internal control.

(F) Band intensities of PDV2 in (E) were quantified and normalized to H3. *GFP-ATG8a* in DMSO (DEX-) was set as 100%.

(G) LIR-SNT-BFP induction did not change the giant chloroplast phenotype in *pdv2*. Five-day-old *pdv2*, *GFP-ATG8a/LIR-SNT-BFP*, and *pdv2/GFP-ATG8a/LIR-SNT-BFP* were treated with DMSO or 10 μM DEX for 10 days. Mesophyll cells from the first pair of true leaves were fixed before confocal imaging. Scale bar, 10 μm.

(H) LIR-SNT-BFP induction did not change the giant chloroplast phenotype in *pdv2*. Cotyledons of 5-day-old seedlings expressing *GFP-ATG8a/LIR-SNT-BFP* in the *pdv2* background, treated with DMSO or 10 μM DEX for 6 days, were analyzed by TEM. Scale bar, 1 μm.

(I) LIR-SNT-BFP induction led to the degradation of chloroplast proteins in *pdv2*. Five-day-old *pdv2/GFP-ATG8a*, *LIR-SNT-BFP/GFP-ATG8a*, and *pdv2/GFP-ATG8a/LIR-SNT-BFP* were treated with DMSO or 10 μM DEX in the presence of 0.5 mM Lin for 14 days before WB detection of chloroplast proteins TOC75 (chloroplast OE protein), TIC40 (IE protein), LHCA1 (Thy protein), RbcL (chloroplast encoded St protein), and RbcS (St protein). Anti-GFP and anti-BFP were used to detect GFP-ATG8a and LIR-SNT-BFP. H3 served as an internal control.

(J) Band intensities in (I) were quantified and normalized to H3. *pdv2/GFP-ATG8a* in DMSO (DEX-) was set as 100%.

Data are means ± SEMs of three biological replicates. *p < 0.05; **p < 0.01; ***p < 0.001; ****p < 0.0001; ns, no significant difference (Student's t test). Representative images or WBs from three biological replicates are shown in (A), (C), (E), and (G)–(I).

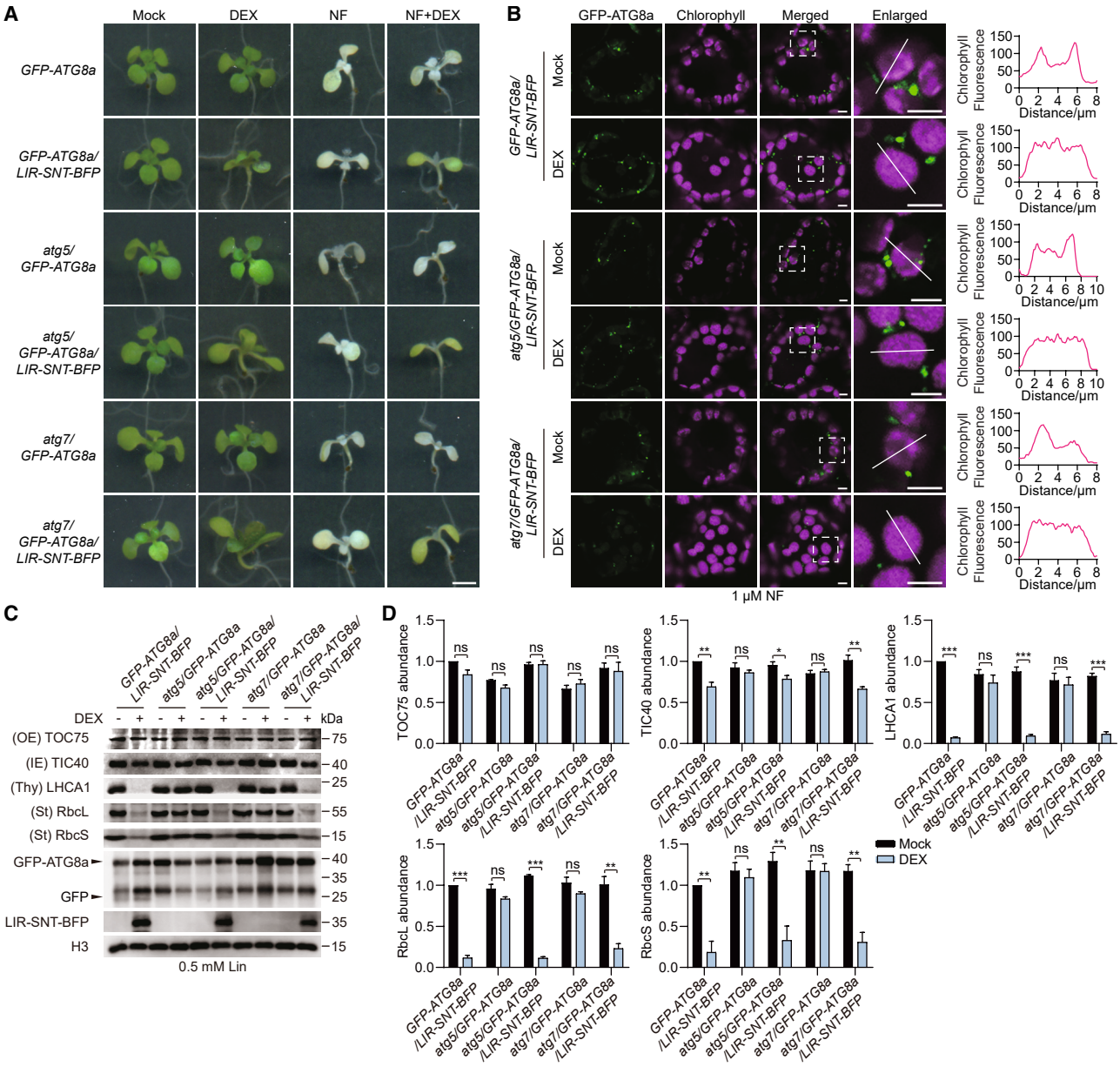

Figure 6. The synthetic receptor-elicited chlorophagy does not require the ATG8 conjugation machinery proteins ATG5 and ATG7

(A) LIR-SNT-BFP induction partially protected cotyledons from chlorosis in NF-treated *atg5* and *atg7*. Five-day-old seedlings expressing *GFP-ATG8a* or *GFP-ATG8a/LIR-SNT-BFP* in the *atg5* or *atg7* background were treated with 10 μM DEX, 1 μM NF, or NF plus DEX for 7 days. Scale bar, 2 mm.

(B) LIR-SNT-BFP induction led to partial recovery of the abnormal, uneven distribution of chlorophyll in NF-treated *atg5* and *atg7*. Five-day-old seedlings expressing *GFP-ATG8a/LIR-SNT-BFP* in the *atg5* or *atg7* background were treated with 1 μM NF, with or without 10 μM DEX for 3 days, before confocal imaging. Chlorophyll fluorescence along the white lines plotted to the right. Scale bar, 5 μm.

(C) LIR-SNT-BFP induction promotes the degradation of chloroplast proteins in *atg5* and *atg7*. Five-day-old seedlings expressing *GFP-ATG8a* or *GFP-ATG8a/LIR-SNT-BFP* in the *atg5* or *atg7* background were treated with DMSO or 10 μM DEX in the presence of 0.5 mM Lin for 14 days before WB detection of chloroplast proteins TOC75 (chloroplast OE protein), TIC40 (IE protein), LHCA1 (Thy protein), RbcL (chloroplast encoded St protein), and RbcS (St protein). Anti-GFP and anti-BFP were used to detect GFP-ATG8a and LIR-SNT-BFP. H3 served as an internal control.

(D) Band intensities in (C) were quantified and normalized to H3. *GFP-ATG8a/LIR-SNT-BFP* in DMSO (DEX-) was set as 100%.

Data are means ± SEMs of three biological replicates. $*p < 0.05$; $**p < 0.01$; $***p < 0.001$; ns, no significant difference (Student's t test). Representative images or WBs from three biological replicates are shown in (A)–(C).

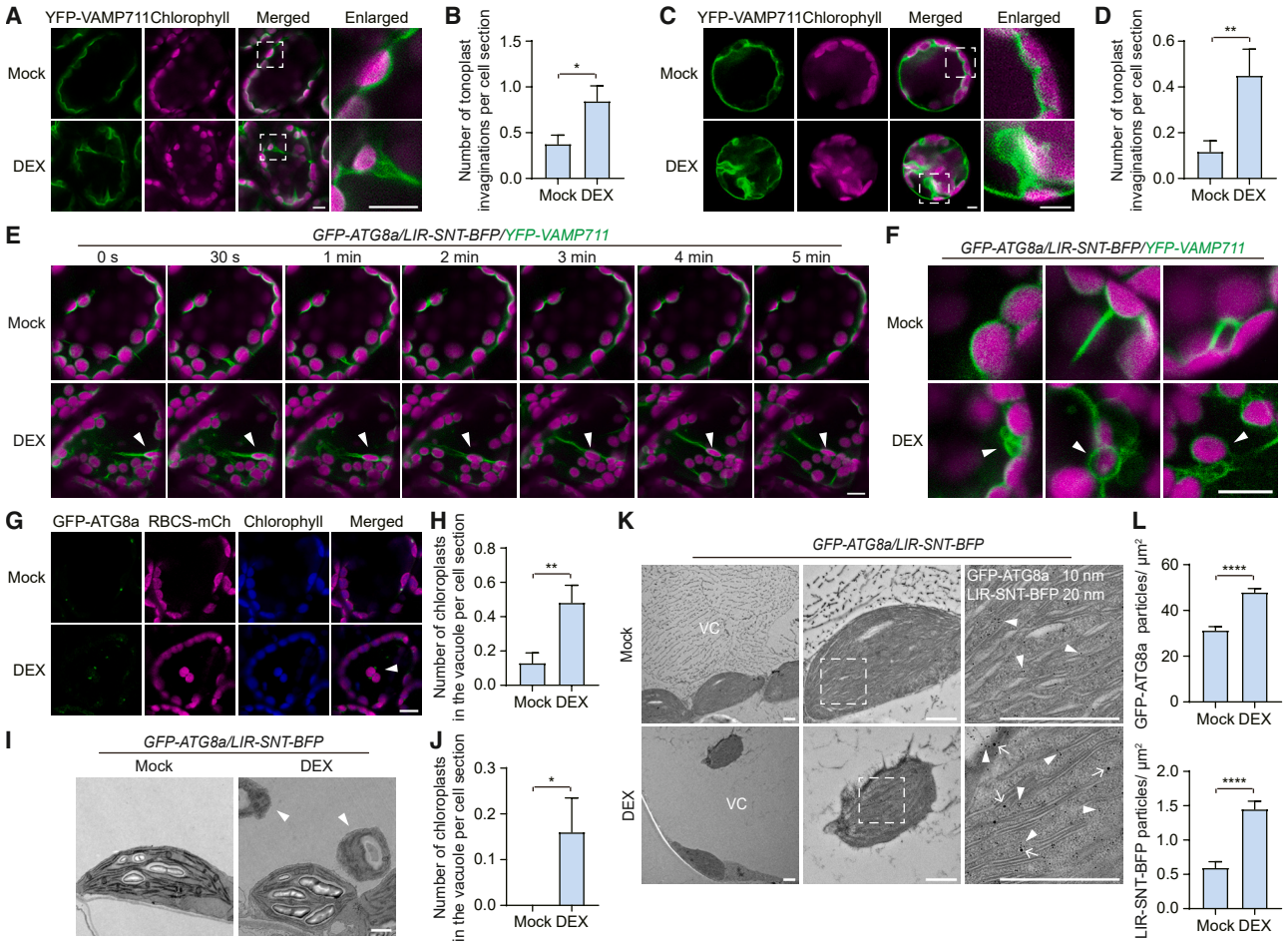

Figure 7. The synthetic receptor-elicited chlorophagy is likely a form of microautophagy

(A) Tonoplast invaginations that wrap chloroplasts were observed after LIR-SNT-BFP induction. Five-day-old seedlings expressing *GFP-ATG8a/LIR-SNT-BFP/YFP-VAMP711* were treated with DMSO or 10 μM DEX for 5 days before confocal imaging. Scale bar, 10 μm.

(B) Quantification of the number of tonoplast invaginations per cell section in (A). Data are means ± SEMs (n = 32).

(C) Tonoplast invaginations that wrap chloroplasts were frequently observed after LIR-SNT-BFP induction in protoplasts. Fourteen-day-old seedlings expressing *GFP-ATG8a/LIR-SNT-BFP/YFP-VAMP711* were treated with DMSO or 30 μM DEX for 12 h, before preparation of protoplasts. Scale bar, 5 μm.

(D) Quantification of the number of tonoplast invaginations per cell section in (C). Data are means ± SEMs (n = 60).

(E) Real-time imaging of tonoplast invagination that wraps chloroplasts (white arrowheads) after LIR-SNT-BFP induction. Five-day-old seedlings expressing *GFP-ATG8a/LIR-SNT-BFP/YFP-VAMP711* were treated with DMSO or 10 μM DEX for 5 days before live-cell imaging. Scale bar, 10 μm.

(F) Chloroplasts wrapped by vacuoles and clusters of small vacuoles (white arrowheads) were observed after LIR-SNT-BFP induction. Cotyledons of *GFP-ATG8a/LIR-SNT-BFP/YFP-VAMP711* plants in (E) were analyzed by confocal imaging. Scale bar, 10 μm.

(G) Chloroplasts are present in the central vacuole after LIR-SNT-BFP induction. Five-day-old seedlings expressing *GFP-ATG8a/LIR-SNT-BFP/RBCS1A-mCherry* were treated with DMSO or 10 μM DEX for 5 days. The V-ATPase inhibitor concanamycin A (1 μM) was added 24 h before confocal imaging. White arrowhead indicates chloroplasts in the vacuole. Scale bar, 10 μm.

(H) Quantification of the number of chloroplasts in the vacuole per cell section in (G). Data are means ± SEMs (n = 54).

(I) Presence of chloroplasts in the central vacuole after LIR-SNT-BFP induction revealed by TEM. Five-day-old seedlings expressing *GFP-ATG8a/LIR-SNT-BFP* were treated with DMSO or 10 μM DEX for 5 days, and the cotyledons were chemically fixed and analyzed by TEM. White arrowheads indicate the chloroplasts in the vacuole. Scale bar, 1 μm.

(J) Quantification of the number of chloroplasts in the vacuole per image in (I). Data are means ± SEMs (n = 25).

(K) Detection of LIR-SNT-BFP and GFP-ATG8a on the chloroplasts in the vacuole by immunoelectron microscopy (IEM). Five-day-old seedlings expressing *GFP-ATG8a/LIR-SNT-BFP* were treated with DMSO or 10 μM DEX for 5 days, and the cotyledons were high-pressure frozen-fixed and analyzed by IEM. The samples were double-immunolabeled with anti-GFP (arrowheads) followed by 10-nm gold-conjugated goat anti-mouse immunoglobulin G (IgG), and anti-BFP (arrows) followed by 20-nm gold-conjugated goat anti-rabbit IgG. Scale bar, 1 μm. VC, vacuole.

(L) Quantification of the number of anti-GFP and anti-BFP gold labeling on chloroplasts in (K). Data are means ± SEM (n = 18).

*p < 0.05; **p < 0.01; ****p < 0.0001; Student's t test. Representative images from three biological replicates are shown in (A), (C), (E)–(G), (I), and (K).

double-label immunoelectron microscopy to examine whether entire chloroplasts in the vacuole observed after DEX treatment were synthetic receptor positive. In the mesophyll cells of DEX-treated *GFP-ATG8a/LIR-SNT-BFP* seedlings, chloroplasts in the vacuole were labeled with both the synthetic receptor LIR-SNT-BFP (larger gold particles, 20 nm in diameter) and GFP-ATG8a (smaller gold particles, 10 nm in diameter) (Figures 7K and 7L). These results suggested that the chloroplasts were indeed degraded in the vacuole by microautophagy elicited by the synthetic receptor.

DISCUSSION

Inducible degradation of whole chloroplasts with an artificial/synthetic receptor: Proof of concept and application potential

Even with over 2 decades of studies on plant autophagy, a canonical chloroplast autophagy receptor that mediates vacuolar degradation of the entire chloroplasts remains unidentified. As a proof of concept, we designed and constructed a chloroplast autophagy receptor that combines OE localization, the ability to recruit ATG8, and a fluorescent protein tag (Figures 1 and S1). With an inducible expression system, this synthetic chlorophagy receptor accumulates only upon DEX treatment and thus may avoid silencing or lethal effects often associated with constitutively elevated chlorophagy. Induced expression of this synthetic receptor simultaneously promotes chloroplast autophagy and division (Figures 2 and 5). Surprisingly, it was a form of microautophagy that we observed, as vacuoles clearly engulfed the chloroplasts (Figure 7; Videos S1–S4). Neither ATG5 nor ATG7 is required for such microautophagy (Figures 6 and S7). Also to our surprise, although chloroplast division evidently accompanies chlorophagy, PDV2, a central organizer of chloroplast division machinery on the cytoplasmic side, is not required for this form of chlorophagy (Figure 5). This is similar to carbon starvation-induced chloroplast piecemeal autophagy, in which DRP5B/ARC5, a dynamin-related protein recruited by PDV2 that constitutes the division ring on the cytoplasmic side,[50] is not required.[16] However, the synthetic receptor-mediated chlorophagy is different from the piecemeal degradation of chloroplasts, for no RCB puncta were detected in the vacuole after the induction of the receptor (Figure 7), and the piecemeal chlorophagy does require ATG5 and ATG7.[16] Hence, both shared and different chloroplast autophagy mechanisms are involved between the two forms of chlorophagy.

Enhanced organelle autophagy, especially mitophagy, is critical to organismal homeostasis, increased fitness, and longevity in animal models.[51,52] Nevertheless, the benefit of organelle autophagy induction has not been fully explored in plants. Using the synthetic chlorophagy receptor, we found that increased chloroplast autophagy can promote plant growth and that a certain upper-level limit for autophagy in promoting plant growth exists, regardless of which transgenic line is examined (Figure 3). Beyond this level, autophagy becomes detrimental and inhibits rosette growth. This, to our knowledge, is the first report on an upper-level limit of plant autophagic flux with respect to optimal growth. Another interesting finding was the partial rescue of herbicide-induced chlorophyll damage and leaf chlorosis with induced chlorophagy (Figure 4). Induced chlorophagy helped alleviate the damage in chlorophyll biosynthesis or electron transport, likely contributing to the homeostasis of the chloroplast population in a mesophyll cell. However, the tolerance to herbicides conferred by artificially induced chlorophagy also appeared to be limited.

What really happens during chloroplast microautophagy?

So far, no canonical chlorophagy receptor has been reported. This synthetic chlorophagy we developed may partially mimic the as-yet unidentified endogenous chlorophagy receptor. We noticed several interesting facts during this specific form of chlorophagy. First, a small population of ATG8 already decorates chloroplast under control condition, as reported.[36] Second, the chlorophagy we observed does not require the ATG8 conjugation machinery. Third, chloroplasts engulfed by vacuoles were observed when the synthetic receptor is induced. Also, we did not see protrusions that shed off chloroplasts like in carbon-starved leaves.[16] We speculated that both endogenous piecemeal autophagy, mediated by phycoerythrin-conjugated ATG8, and microautophagy of the entire chloroplasts may have taken place. The dramatic change in vacuole shape around the chloroplast is somewhat similar to early observations on peroxisome degradation by microautophagy.[53] When shifted from methanol medium to glucose medium, *Pichia pastoris* (*Komagataella phaffii*) and *Hansenula polymorpha*, two methylotrophic yeast species, would promptly degrade their enlarged peroxisomes that had been metabolizing methanol as a carbon source. The large size of chloroplasts and vacuoles can be compared to the large size of peroxisomes and vacuoles in the two yeast species, and some mechanisms may be shared between these forms of microautophagy. For instance, the ATG8 cluster on chloroplasts may represent a structure similar to micropexophagy-specific membrane apparatus in *P. pastoris*, and the clustered vacuoles may be similar to vacuolar sequestering membrane, which facilitates microautophagy of large organelles. The detailed molecular mechanism, however, remains to be explored.

In summary, targeted degradation of a large organelle, the chloroplast, is achieved with an inducible synthetic autophagy receptor. The beneficial effects of moderately induced chloroplast autophagy included increased rosette size and partial protection against the herbicides NF and DCMU. Both are potentially useful for crop breeding. With this tool, we also uncovered interesting behaviors of chloroplasts and vacuoles, such as PDV2-independent chlorophagy, and microautophagy that appears independent of ATG8 lipidation.

Limitations of the study

We recognize two main limitations of this study. First, we did not fully explore the effects of the induced chlorophagy on seed yield. This was mainly because long-term, consecutive DEX treatment was not easy to achieve. Second, the molecular mechanism for chloroplast microautophagy remains unknown. The fact that we cannot recover the synthetic chlorophagy receptor in the *atg2* background suggests that ATG2 is a critical component in chloroplast microautophagy. Whether it regulates

the homotypic fusion of vacuoles, which are not easy to observe in real time and hard to recapture *in vitro* is currently unknown.

RESOURCE AVAILABILITY

Lead contact

Further information and requests for resources and reagents should be directed to and will be fulfilled by the lead contact, Qingqiu Gong (gongqingqiu@sjtu.edu.cn).

Materials availability

All plant materials and plasmids generated in this study are available from the lead contact upon request. This study did not generate new unique reagents.

Data and code availability

- All data reported in this paper will be shared by the lead contact upon request.
- This paper does not report original code.
- Any additional information required to reanalyze the data reported in this paper is available from the lead contact upon request.

ACKNOWLEDGMENTS

We thank Cheng Chen (Shanghai Jiao Tong University) for the *pdv2* seeds, Hongbo Gao (Beijing Forestry University) for the PDV2 antibody, and Qihua Ling (Institute of Plant Physiology and Ecology, Chinese Academy of Sciences) for the anti-TOC75 antibody. We thank Dr. Yu Kong and Xu Wang (Electron Microscopy Facilities of Center for Excellence in Brain Science and Technology, Chinese Academy of Science) and the electron microscopy center of Shanghai Institute of Precision Medicine, Shanghai Ninth People's Hospital, Shanghai Jiao Tong University School of Medicine for their assistance in immunoelectron microscopy sample preparation and image analysis. We thank Cheng Chen, Hongbo Gao, Qihua Ling, Quan-Sheng Qiu (Lanzhou University), Zhiping Xie (Shanghai Jiao Tong University), Heng Zhang (Shanghai Jiao Tong University), and Xin-Guang Zhu (Institute of Plant Physiology and Ecology, Chinese Academy of Sciences) for suggestions, and our lab members for discussions. This work was supported by grants from the National Natural Science Foundation of China (grant nos. 32270726, 92354302, 91954102, and 31871355) and the Natural Science Foundation of Shanghai (grant no. 23ZR1429400) to Q.G. T.W. is supported by Startup Fund for Young Faculty at Shanghai Jiao Tong University.

AUTHOR CONTRIBUTIONS

Q.G. initiated the project. R.L. performed most of the experiments. X.W., X.L., Y.C., Q.L., L.L., and D.T. performed some of the experiments. R.L., T.W., H.W., Z.K., and Q.G. analyzed the data. R.L. and Q.G. drafted the paper. Q.G. edited the paper. T.W. and Q.G. acquired the funding. H.W., Z.K., and Q.G. supervised the study.

DECLARATION OF INTERESTS

The authors declare no competing interests.

STAR★METHODS

Detailed methods are provided in the online version of this paper and include the following:

SUPPLEMENTAL INFORMATION

Supplemental information can be found online at https://doi.org/10.1016/j.celrep.2025.115759.

Received: May 29, 2024
Revised: April 7, 2025
Accepted: May 8, 2025
Published: May 30, 2025

REFERENCES

1. Raffeiner, M., Zhu, S., González-Fuente, M., and Üstün, S. (2023). Interplay between autophagy and proteasome during protein turnover. Trends Plant Sci. *28*, 698–714.
2. Gubas, A., and Dikic, I. (2022). A Guide To The regulation of selective autophagy receptors. FEBS J. *289*, 75–89.
3. Yan, H., Qi, A., Lu, Z., You, Z., Wang, Z., Tang, H., Li, X., Xu, Q., Weng, X., Du, X., et al. (2024). Dual roles of AtNBR1 in regulating selective autophagy via liquid-liquid phase separation and recognition of non-ubiquitinated substrates in Arabidopsis. Autophagy *20*, 2804–2815.
4. Noda, N.N., Ohsumi, Y., and Inagaki, F. (2010). Atg8-family interacting motif crucial for selective autophagy. FEBS Lett. *584*, 1379–1385.
5. Rogov, V.V., Nezis, I.P., Tsapras, P., Zhang, H., Dagdas, Y., Noda, N.N., Nakatogawa, H., Wirth, M., Mouilleron, S., McEwan, D.G., et al. (2023). Atg8 family proteins, LIR/AIM motifs and other interaction modes. Autophagy Rep. *2*, 27694127.2023.2188523.
6. Yamamoto, H., Zhang, S., and Mizushima, N. (2023). Autophagy genes in biology and disease. Nat. Rev. Genet. *24*, 382–400.
7. Li, Z., Wang, C., Wang, Z., Zhu, C., Li, J., Sha, T., Ma, L., Gao, C., Yang, Y., Sun, Y., et al. (2019). Allele-selective lowering of mutant HTT protein by HTT-LC3 linker compounds. Nature *575*, 203–209.
8. Tan, S., Wang, D., Fu, Y., Zheng, H., Liu, Y., and Lu, B. (2023). Targeted clearance of mitochondria by an autophagy-tethering compound (ATTEC) and its potential therapeutic effects. Sci. Bull. *68*, 3013–3026.
9. Takahashi, D., Moriyama, J., Nakamura, T., Miki, E., Takahashi, E., Sato, A., Akaike, T., Itto-Nakama, K., and Arimoto, H. (2019). AUTACs: Cargo-Specific Degraders Using Selective Autophagy. Mol. Cell *76*, 797–810.e10.
10. Ji, C.H., Kim, H.Y., Lee, M.J., Heo, A.J., Park, D.Y., Lim, S., Shin, S., Ganipisetti, S., Yang, W.S., Jung, C.A., et al. (2022). The AUTOTAC chemical biology platform for targeted protein degradation via the autophagy-lysosome system. Nat. Commun. *13*, 904.
11. Mei, L., Chen, X., Wei, F., Huang, X., Liu, L., Yao, J., Chen, J., Luo, X., Wang, Z., and Yang, A. (2023). Tethering ATG16L1 or LC3 induces targeted autophagic degradation of protein aggregates and mitochondria. Autophagy *19*, 2997–3013.
12. Luo, N., Shang, D., Tang, Z., Mai, J., Huang, X., Tao, L.Z., Liu, L., Gao, C., Qian, Y., Xie, Q., and Li, F. (2023). Engineered ATG8-binding motif-based selective autophagy to degrade proteins and organelles. New Phytol. *237*, 684–697.
13. Izumi, M., and Nakamura, S. (2018). Chloroplast Protein Turnover: The Influence of Extraplastidic Processes, Including Autophagy. Int. J. Mol. Sci. *19*, 828.
14. Zhuang, X., and Jiang, L. (2019). Chloroplast Degradation: Multiple Routes Into the Vacuole. Front. Plant Sci. *10*, 359.

15. Ishida, H., Yoshimoto, K., Izumi, M., Reisen, D., Yano, Y., Makino, A., Ohsumi, Y., Hanson, M.R., and Mae, T. (2008). Mobilization of rubisco and stroma-localized fluorescent proteins of chloroplasts to the vacuole by an ATG gene-dependent autophagic process. Plant Physiol. *148*, 142–155.

16. Izumi, M., Nakamura, S., Otomo, K., Ishida, H., Hidema, J., Nemoto, T., and Hagihara, S. (2024). Autophagosome development and chloroplast segmentation occur synchronously for piecemeal degradation of chloroplasts. Elife *12*, RP93232.

17. Wang, Y., Yu, B., Zhao, J., Guo, J., Li, Y., Han, S., Huang, L., Du, Y., Hong, Y., Tang, D., and Liu, Y. (2013). Autophagy Contributes to Leaf Starch Degradation. Plant Cell *25*, 1383–1399.

18. Michaeli, S., Honig, A., Levanony, H., Peled-Zehavi, H., and Galili, G. (2014). ATG8-INTERACTING PROTEIN1 Is Involved in Autophagy-Dependent Vesicular Trafficking of Plastid Proteins to the Vacuole. Plant Cell *26*, 4084–4101.

19. Izumi, M., Ishida, H., Nakamura, S., and Hidema, J. (2017). Entire Photodamaged Chloroplasts Are Transported to the Central Vacuole by Autophagy. Plant Cell *29*, 377–394.

20. Wada, S., Ishida, H., Izumi, M., Yoshimoto, K., Ohsumi, Y., Mae, T., and Makino, A. (2009). Autophagy plays a role in chloroplast degradation during senescence in individually darkened leaves. Plant Physiol. *149*, 885–893.

21. Ono, Y., Wada, S., Izumi, M., Makino, A., and Ishida, H. (2013). Evidence for contribution of autophagy to rubisco degradation during leaf senescence in Arabidopsis thaliana. Plant Cell Environ. *36*, 1147–1159.

22. Nakamura, S., Hidema, J., Sakamoto, W., Ishida, H., and Izumi, M. (2018). Selective Elimination of Membrane-Damaged Chloroplasts via Microautophagy. Plant Physiol. *177*, 1007–1026.

23. Lemke, M.D., Fisher, K.E., Kozlowska, M.A., Tano, D.W., and Woodson, J. D. (2021). The core autophagy machinery is not required for chloroplast singlet oxygen-mediated cell death in the Arabidopsis thaliana plastid ferrochelatase two mutant. BMC Plant Biol. *21*, 342.

24. Lee, H.N., Chacko, J.V., Solis, A.G., Chen, K.E., Barros, J.A., Signorelli, S., Millar, A.H., Vierstra, R.D., Eliceiri, K.W., Otegui, M.S., et al. (2023). The autophagy receptor NBR1 directs the clearance of photodamaged chloroplasts. Elife *12*, e86030.

25. Kikuchi, Y., Nakamura, S., Woodson, J.D., Ishida, H., Ling, Q., Hidema, J., Jarvis, R.P., Hagihara, S., and Izumi, M. (2020). Chloroplast Autophagy and Ubiquitination Combine to Manage Oxidative Damage and Starvation Responses. Plant Physiol. *183*, 1531–1544.

26. Otegui, M.S., Noh, Y.S., Martínez, D.E., Vila Petroff, M.G., Staehelin, L.A., Amasino, R.M., and Guiamet, J.J. (2005). Senescence-associated vacuoles with intense proteolytic activity develop in leaves of Arabidopsis and soybean. Plant J. *41*, 831–844.

27. Martinez, D.E., Costa, M.L., Gomez, F.M., Otegui, M.S., and Guiamet, J.J. (2008). Senescence-associated vacuoles' are involved in the degradation of chloroplast proteins in tobacco leaves. Plant J. *56*, 196–206.

28. Carrión, C.A., Costa, M.L., Martínez, D.E., Mohr, C., Humbeck, K., and Guiamet, J.J. (2013). inhibition of cysteine proteases provides evidence for the involvement of 'senescence-associated vacuoles' in chloroplast protein degradation during dark-induced senescence of tobacco leaves. J. Exp. Bot. *64*, 4967–4980.

29. Wang, S., and Blumwald, E. (2014). Stress-induced chloroplast degradation in Arabidopsis is regulated via a process independent of autophagy and senescence-associated vacuoles. Plant Cell *26*, 4875–4888.

30. Žnidarič, M.T., Zagorščak, M., Ramšak, Ž., Stare, K., Chersicola, M., Novak, M.P., Kladnik, A., and Dermastia, M. (2025). Chloroplast Vesiculation and Induced Chloroplast Vesiculation and Senescence-Associated Gene 12 Expression During Tomato Flower Pedicel Abscission. Plant Direct *9*, e70035.

31. Pan, T., Liu, Y., Hu, X., Li, P., Lin, C., Tang, Y., Tang, W., Liu, Y., Guo, L., Kim, C., et al. (2023). Stress-induced endocytosis from chloroplast inner envelope membrane is mediated by CHLOROPLAST VESICULATION but inhibited by GAPC. Cell Rep. *42*, 113208.

32. Svenning, S., Lamark, T., Krause, K., and Johansen, T. (2011). Plant NBR1 is a selective autophagy substrate and a functional hybrid of the mammalian autophagic adapters NBR1 and p62/SQSTM1. Autophagy *7*, 993–1010.

33. Fourrier, N., Bédard, J., Lopez-Juez, E., Barbrook, A., Bowyer, J., Jarvis, P., Warren, G., and Thorlby, G. (2008). A role for SENSITIVE TO FREEZING2 in protecting chloroplasts against freeze-induced damage in Arabidopsis. Plant J. *55*, 734–745.

34. Aoyama, T., and Chua, N.H. (1997). A glucocorticoid-mediated transcriptional induction system in transgenic plants. Plant J. *11*, 605–612.

35. Luo, L., Zhang, P., Zhu, R., Fu, J., Su, J., Zheng, J., Wang, Z., Wang, D., and Gong, Q. (2017). Autophagy Is Rapidly Induced by Salt Stress and Is Required for Salt Tolerance in Arabidopsis. Front. Plant Sci. *8*, 1459.

36. Wan, C., Zhang, H., Cheng, H., Sowden, R.G., Cai, W., Jarvis, R.P., and Ling, Q. (2023). Selective autophagy regulates chloroplast protein import and promotes plant stress tolerance. Embo j *42*, e112534.

37. Linnane, A.W., and Stewart, P.R. (1967). The inhibition of chlorophyll formation in Euglena by antibiotics which inhibit bacterial and mitochondrial protein synthesis. Biochem. Biophys. Res. Commun. *27*, 511–516.

38. Park, J.H., Tran, L.H., and Jung, S. (2017). Perturbations in the Photosynthetic Pigment Status Result in Photooxidation-Induced Crosstalk between Carotenoid and Porphyrin Biosynthetic Pathways. Front. Plant Sci. *8*, 1992.

39. Ridley, S.M. (1977). Interaction of Chloroplasts with Inhibitors - Induction of Chlorosis by Diuron during Prolonged Illumination Invitro. Plant Physiol. *59*, 724–732.

40. Frank, M., Duvezin-Caubet, S., Koob, S., Occhipinti, A., Jagasia, R., Petcherski, A., Ruonala, M.O., Priault, M., Salin, B., and Reichert, A.S. (2012). Mitophagy is triggered by mild oxidative stress in a mitochondrial fission dependent manner. Bba-Mol Cell Res *1823*, 2297–2310.

41. Fukuda, T., Furukawa, K., Maruyama, T., Yamashita, S.I., Noshiro, D., Song, C., Ogasawara, Y., Okuyama, K., Alam, J.M., Hayatsu, M., et al. (2023). The mitochondrial intermembrane space protein mitofissin drives mitochondrial fission required for mitophagy. Mol. Cell *83*, 2045–2058.e9.

42. Osteryoung, K.W., Stokes, K.D., Rutherford, S.M., Percival, A.L., and Lee, W.Y. (1998). Chloroplast division in higher plants requires members of two functionally divergent gene families with homology to bacterial ftsZ. Plant Cell *10*, 1991–2004.

43. Okazaki, K., Kabeya, Y., Suzuki, K., Mori, T., Ichikawa, T., Matsui, M., Nakanishi, H., and Miyagishima, S.Y. (2009). The PLASTID DIVISION1 and 2 components of the chloroplast division machinery determine the rate of chloroplast division in land plant cell differentiation. Plant Cell *21*, 1769–1780.

44. Chang, N., Sun, Q., Li, Y., Mu, Y., Hu, J., Feng, Y., Liu, X., and Gao, H. (2017). PDV2 has a dosage effect on chloroplast division. Plant Cell Rep. *36*, 471–480.

45. Okazaki, K., Kabeya, Y., Suzuki, K., Mori, T., Ichikawa, T., Matsui, M., Nakanishi, H., and Miyagishima, S.Y. (2009). The PLASTID DIVISION1 and 2 Components of the Chloroplast Division Machinery Determine the Rate of Chloroplast Division in Land Plant Cell Differentiation. Plant Cell *21*, 1769–1780.

46. Miyagishima, S.Y., Froehlich, J.E., and Osteryoung, K.W. (2006). PDV1 and PDV2 mediate recruitment of the dynamin-related protein ARC5 to the plastid division site. Plant Cell *18*, 2517–2530.

47. Luo, M.Q., Law, K.C., He, Y.L., Chung, K.K., Po, M.K., Feng, L.L., Chung, K.P., Gao, C.J., Zhuang, X.H., and Jiang, L.W. (2023). Arabidopsis AUTOPHAGY-RELATED2 is essential for ATG18a and ATG9 trafficking during autophagosome closure. Plant Physiol *193*, 304–321.

48. Thompson, A.R., Doelling, J.H., Suttangkakul, A., and Vierstra, R.D. (2005). Autophagic nutrient recycling in Arabidopsis directed by the ATG8 and ATG12 conjugation pathways. Plant Physiol. *138*, 2097–2110.

49. Geldner, N., Dénervaud-Tendon, V., Hyman, D.L., Mayer, U., Stierhof, Y. D., and Chory, J. (2009). Rapid, combinatorial analysis of membrane compartments in intact plants with a multicolor marker set. Plant J. *59*, 169–178.

50. Liu, M., Yu, J., Yang, M., Cao, L., and Chen, C. (2024). Adaptive evolution of chloroplast division mechanisms during plant terrestrialization. Cell Rep. *43*, 113950.

51. Chen, G., Kroemer, G., and Kepp, O. (2020). Mitophagy: An Emerging Role in Aging and Age-Associated Diseases. Front. Cell Dev. Biol. *8*, 200.

52. Klionsky, D.J., Petroni, G., Amaravadi, R.K., Baehrecke, E.H., Ballabio, A., Boya, P., Bravo-San Pedro, J.M., Cadwell, K., Cecconi, F., Choi, A.M.K., et al. (2021). Autophagy in major human diseases. Embo J *40*, e108863.

53. Sakai, Y., Koller, A., Rangell, L.K., Keller, G.A., and Subramani, S. (1998). Peroxisome degradation by microautophagy in Pichia pastoris: identification of specific steps and morphological intermediates. J. Cell Biol. *141*, 625–636.

54. Liu, R., Zhang, R., Yang, Y., Liu, X., and Gong, Q. (2022). Monitoring Autophagy in Rice With GFP-ATG8 Marker Lines. Front. Plant Sci. *13*, 866367.

55. Yue, M., Hu, B., Li, J., Chen, R., Yuan, Z., Xiao, H., Chang, H., Jiu, Y., Cai, K., and Ding, B. (2023). Coronaviral ORF6 protein mediates inter-organelle contacts and modulates host cell lipid flux for virus production. EMBO J. *42*, e112542.

STAR★METHODS

KEY RESOURCES TABLE

REAGENT or RESOURCE	SOURCE	IDENTIFIER
Antibodies		
Rabbit anti-tRFP	Evrogen	Cat#AB233; RRID:AB_2571743
Mouse anti-GFP	Utibody	Cat#UM3002
Mouse anti-Tubulin	Utibody	Cat#UM4003
Rabbit anti-Histone H3.1	Abmart	Cat#P30266; RRID:AB_2936509
Mouse anti-Rubisco (1A11)	Abmart	Cat#M20043
Rabbit anti-RbcS	Orizymes	Cat#PAB07002
Rabbit anti-LHCA1	Orizymes	Cat#PAB05001
Rabbit anti-TIC40	Agrisera	Cat#AS10709; RRID:AB_10748384
Rabbit anti-TOC75	Gifted by Qihua Lin, Institute of Plant Physiology and Ecology, Chinese Academy of Sciences	N/A
Rabbit anti-PDV2	Gifted by Hongbo Gao, Beijing Forestry University	N/A
Bacterial and virus strains		
DH5α	N/A	N/A
GV3101	N/A	N/A
Chemicals, peptides, and recombinant proteins		
Hygromycin B	Roche	Cat#10843555001
Basta	BBI	Cat#A614229-0100
Dexamethasone	MERYER	Cat#M17752-5G
Lincomycin	BBI	Cat#A600604-0025
Diuron	Sigma-Aldrich	Cat#45463-250MG
Norflurazon	Dr. Ehrenstorfer	Cat# CDCT-C15650000
Critical commercial assays		
ClonExpress II One Step Cloning Kit	Vazyme	Cat#C112-01
ClonExpress MultiS One Step Cloning Kit	Vazyme	Cat#C113-01
LinBio Supersensitive ECL kit	LINDE	Cat#LP200202
Experimental models: Organisms/strains		
Arabidopsis, Col-0 wild-type	This paper	N/A
Arabidopsis, atg2-1	ABRC	SALK_076727
Arabidopsis, atg5-1	ABRC	CS806267
Arabidopsis, atg7	ABRC	CS862226
Arabidopsis, pdv2-1	Gifted by Cheng Chen, Shanghai Jiao Tong University	SALK_059656
Arabidopsis, ProUBQ10:GFP-ATG8a	Luo et al.[31]	N/A
Arabidopsis, ProUBQ10:GFP-ATG8a/GVG:BFP	This paper	N/A
Arabidopsis, ProUBQ10:GFP-ATG8a/GVG:SNT-BFP	This paper	N/A
Arabidopsis, ProUBQ10:GFP-ATG8a/GVG:LIR-SNT-BFP	This paper	N/A
Arabidopsis, ProUBQ10:GFP-ATG8a/GVG:SNT-BFP-LIR	This paper	N/A
Arabidopsis, ProUBQ10:GFP-ATG8a/GVG:LIR-SNT-BFP/YFP-VAMP711	This paper	N/A

(*Continued on next page*)

Continued

REAGENT or RESOURCE	SOURCE	IDENTIFIER
Arabidopsis, ProUBQ10:GFP-ATG8a/GVG: LIR-SNT-BFP/pdv2	This paper	N/A
Arabidopsis, ProUBQ10:GFP-ATG8a/pdv2	This paper	N/A
Arabidopsis, ProUBQ10:GFP-ATG8a/GVG: LIR-SNT-BFP/atg2	This paper	N/A
Arabidopsis, ProUBQ10:GFP-ATG8a/atg2	This paper	N/A
Arabidopsis, ProUBQ10:GFP-ATG8a/GVG: LIR-SNT-BFP/atg5	This paper	N/A
Arabidopsis, ProUBQ10:GFP-ATG8a/atg5	This paper	N/A
Arabidopsis, ProUBQ10:GFP-ATG8a/GVG: LIR-SNT-BFP/atg7	This paper	N/A
Arabidopsis, ProUBQ10:GFP-ATG8a/atg7	This paper	N/A
Arabidopsis, ProUBQ10:GFP-ATG8a/GVG: LIR-SNT-BFP/ProRBCS1A:RBCS1A-mCherry	This paper	N/A
Oligonucleotides		
Primers are listed in Table S1	This paper	N/A
Recombinant DNA		
ProUBQ10:GFP-ATG8a	This paper	N/A
ProUBQ10:BFP	This paper	N/A
ProUBQ10:LIR-SNT-BFP	This paper	N/A
GVG:LIR-SNT-BFP	This paper	N/A
GVG:SNT-BFP-LIR	This paper	N/A
GVG:SNT-BFP	This paper	N/A
GVG:BFP	This paper	N/A
Software and algorithms		
GraphPad Prism 9	GraphPad Software, USA	https://www.graphpad.com/scientific-software/prism/
ImageJ	NIH, USA	https://imagej.nih.gov/
Adobe Illustrator 2023	Adobe	N/A

EXPERIMENTAL MODEL AND STUDY PARTICIPANT DETAILS

Plant materials and growth conditions

Arabidopsis thaliana used in this study was in Columbia-0 (Col-0) background. The transfer DNA insertion mutants of *atg2-1* (SALK_076727), *atg5-1* (SAIL_129B07, CS806267), and *atg7* (SAIL_11H07, CS862226), were obtained from ABRC. *pdv2-1* (SALK_059656) was a gift from Cheng Chen (Shanghai Jiao Tong University). All the other plant materials used in this study were generated by crossing or floral dipping. Surface-sterilized Arabidopsis seeds were stratified at 4°C for 2 days in the dark. Transgenic plants expressing *GFP-ATG8a* were selected on half-strength Murashige and Skoog (1/2 MS) medium containing 20 mg/mL Hygromycin B. Transgenic plants co-expressing *LIR-SNT-BFP* and *GFP-ATG8a* were selected on 1/2 MS medium containing 20 mg/mL Hygromycin B and Basta (1:10000 dilution). Transgenic plants expressing *GFP-ATG8a/LIR-SNT-BFP/RBCS1A-mCherry* were selected on 1/2 MS medium containing 20 mg/mL Hygromycin B, 50 mg/mL Kana and Basta (1:10000 dilution).For DEX treatment, five-day-old seedlings were transferred to 1/2 MS medium supplemented with DMSO or 10 μM DEX. Plants were grown at 16 h (22°C)/8 h (18°C) with full spectrum LED lamps at 100 $\mu E\ m^{-2}\ s^{-1}$. Primers used for genotyping are listed in Table S1.

METHOD DETAILS

Plasmids construction

The synthetic chlorophagy receptor LIR-SNT-BFP contains the LIR domain of AtNBR1 (LIR, aa633-687) to interact with ATG8, the N-terminal of AtSFR2 (SNT, aa1-31) to localize to the chloroplast outer envelope, and a BFP. For inducible expression of the receptor, a *pCAMBIA3301* vector carrying *GVG* (a glucocorticoid receptor-based inducible gene expression system) was constructed. The *GVG* gene is composed of the *CaMV 35S* promoter, *GAL4*-binding domain-*VP16* activation domain-*GR* fusion, the *rbcS-E9*

terminator and upstream activation sequence (*UAS*), which were amplified from the *pTA7002* vector. Then the *LIR-SNT-BFP* fusion gene was inserted between Nco I and Eco91 I of *pCAMBIA3301*, in frame after *GVG* gene. Primers used for plasmid construction are listed in Table S1.

Transient expression assays

For transient transformation of tobacco leaf epidermal cells, *BFP* or *LIR-SNT-BFP* and *GFP-ATG8a* were introduced into *pCAMBIA1302* vector under the *UBQ10* promoter. Soil-grown, 4-week-old *N. benthamiana* leaves were used for transient transformation. After two days of Agrobacterium inoculation, leaves were collected and cut into small squares for confocal microscopy. For transient transformation of Arabidopsis protoplasts, *BFP* or *LIR-SNT-BFP* were introduced into *pMD19* vector under the *UBQ10* promoter. Soil-grown, three-week-old transgenic Arabidopsis expressing *GFP-ATG8a* were used for preparing protoplasts. Transformation was done as described.[54]

Laser Scanning confocal microscopy (LSCM)

Lower epidermis of transformed *N.benthamiana* leaves, cotyledons of transgenic Arabidopsis seedlings and Arabidopsis protoplasts were observed with a Ni-E A1 HD25 confocal microscope (Nikon, Japan) and an STELLARIS 5 confocal microscope (Leica, Germany). Prior to image collection, the background auto-fluorescence was eliminated using untransformed samples. The BFP fluorescence signal was exited at 405 nm and emission was collected at 425–475 nm. The GFP fluorescence signal was exited at 488 nm and collected at 500–550 nm. The YFP fluorescence signal was exited at 514 nm and collected at 525–555 nm. The mCherry fluorescence signal was exited at 561 nm and collected at 575–620 nm. The chlorophyll auto-fluorescence was exited with 640 nm laser and collected at 650–750 nm.

Chloroplast isolation

Chloroplast isolation from Arabidopsis seedlings was performed as previously described.[36] The chloroplasts were isolated from protoplasts through 40% and 85% Percoll step gradient, washed once with HEPES-sorbitol buffer, and processed for SDS-PAGE analysis.

Immunoblotting and Co-immunoprecipitation

Protein extraction and immunoblotting were done as described.[35] Semi-quantification of the protein levels was performed with ImageJ (https://imagej.nih.gov/) and protein levels were normalized to the H3. For immunoblotting, rabbit anti-H3 (1:8000 dilution, Abmart, China), mouse anti-GFP (1:5,000 dilution, Utibody, China), rabbit anti-BFP/tRFP (1:5000 dilution, Evrogen, Russia), mouse anti-RbcL (1:5000 dilution, Abmart, China), rabbit anti-RbcS (1:5000 dilution, Orizymes, China), rabbit anti-LHCA1 (1:5000 dilution, Orizymes, China), rabbit anti-Tic40 (1:2000 dilution, Agrisera, SWEDEN), rabbit anti-Toc75 (1:1000 dilution, gifted from Qihua Lin), rabbit anti-PDV2 (1:5000 dilution, gifted from Hongbo Gao), and the appropriate IgG-HRP conjugated secondary antibody (1:5000; ZSGB-Bio, China) were used. The signal was developed using Highly Sensitive ECL Chemiluminescence Substrate (LINDE, China) and chemiluminescence was detected using a chemiluminescent Western Blot scanner (ChemiScope 6100T, Clinx, China). All experiments were repeated at least three times with one representative result shown.

For co-immunoprecipitation, transgenic Arabidopsis co-expressing GFP-ATG8a and BFP-tagged proteins were used. Proteins were extracted with IP lysis buffer (50 mM Tris-HCl, pH 7.5, 150 mM NaCl, 1 mM $MgCl_2$, 20% glycerol, 0.2% NP-40, and 1× protease inhibitor), and then centrifuged at 12000 rpm at 4°C for 10 min. The supernatant was incubated with GFP-beads for 3 h at 4°C with slow rotation. After three washes with washing buffer (50 mM Tris-HCl, pH 7.5, 150 mM NaCl, 1 mM $MgCl_2$, 20% glycerol, 0.01% NP-40), bound proteins were eluted by boiling in SDS–PAGE loading buffer for immunoblotting.

Measurement of the number of chloroplasts

First leaves of Arabidopsis seedlings were fixed in 3.5% (v/v) glutaraldehyde for 1 h in the dark and softened in 0.1 M Na_2EDTA (pH 9) at 60°C for 3 h. DIC images were observed using a Ni-E A1 HD25 confocal microscope (Nikon, Japan).

Chlorophyll measurements

Fresh leaves of Arabidopsis seedlings were collected, snap frozen and ground with liquid nitrogen. The powder was mixed with 80% acetone and incubated in the dark for 15–30 min. Cell debris was pelleted three times at 12,000 × g for 15 min at 4°C. The absorbance (A) of chlorophyll content was measured spectrophotometrically using 80% acetone as a blank control. The chlorophyll concentrations are calculated as follows: Chlorophyll *a* (mg/g) = [12.7 × A663–2.69 × A645] × V/W, Chlorophyll *b* (mg/g) = [22.9 × A645–4.86 × A663] × V/W, Chlorophyll *a*+*b* (mg/g) = [8.02 × A663 + 20.20 × A645] × V/W, Where V = volume of the extract (mL); W = weight of fresh leaves (mg).

Transmission electron microscope (TEM)

Cotyledons of transgenic seedlings were fixed with 2.5% (v/v) glutaraldehyde overnight. Then samples were rinsed with 0.1 M phosphate buffer (Na_2HPO_4, NaH_2PO_4) and post-fixed with 1% OsO_4 (w/v) for 2 h at 4°C. Following dehydration with alcohol and acetone series, samples were embedded in EPON 812 (Ted pella, USA) for 2 days at 60°C. Ultrathin sections (thickness 90 nm) were cut with a

Leica EM UC7 (Leica, Germany), mounted on copper grids and contrasted with TI Blue stainer (Nisshin EM, Japan) and 3% lead citrate solution. The sections were examined with a Tecnai G2 spirit BioTWIN transmission electron microscope (FEI, USA) at 120 kV accelerating voltage.

Immunogold electron microscopy (IEM)

Cotyledons of transgenic seedlings were frozen in a high-pressure freezer (Leica EM Ice) and freeze-substituted in acetone contained 0.2% uranyl acetate at −90°C in an automated freeze-substitution device (Leica EM AFS2) for 48 h. The temperature was raised to −50°C in 4 h. After another 12 h of incubation, the temperature was raised to −30°C in 4 h. After another 2 h incubation, the samples were rinsed with pure acetone three times (15 min each) and infiltrated with 25%, 50%, 75%, and 100% HM20 resin at −30°C (2 h each). After infiltrated in pure resin overnight, the samples were embedded in gelatin capsules and polymerized under UV light for 48 h at −30°C and then 12 h at 25°C. The ultrathin sections (100 nm) were prepared and transferred to nickel grids. Double-immunogold labeling was performed as previously described.[55] Primary antibodies (anti-GFP and anti-BFP) were diluted 1:100. Gold particle coupled secondary anti-Mouse (10 nm) and anti-Rabbit (20 nm) antibodies were diluted 1:50. Ultrathin sections were examined using a transmission electron microscope (Thermo Fisher/FEI Talos L 120C).

QUANTIFICATION AND STATISTICAL ANALYSIS

Statistical analyses were performed using Student's t-test. *, **, ***, ****, indicate significant difference with $p < 0.05$, $p < 0.01$, $p < 0.001$ and $p < 0.0001$, respectively. All data were presented as mean ± SE of at least three replicates, as indicated in the figure legends.